

Received June 23, 2021, accepted July 12, 2021, date of publication July 15, 2021, date of current version July 23, 2021.

Digital Object Identifier 10.1109/ACCESS.2021.3097444

# Joint Detection and Decoding of Mixed-ADC Large-Scale MIMO Communication Systems With Protograph LDPC Codes

HUNG N. DANG<sup>1</sup>, HIEU T. NGUYEN<sup>2</sup>, AND THUY V. NGUYEN<sup>1</sup>

<sup>1</sup>Faculty of Information Technology, Posts and Telecommunications Institute of Technology, Hanoi 10000, Vietnam

<sup>2</sup>Department of Science and Industry Systems, Faculty of Technology, Natural Sciences and Maritime Sciences, University of South-Eastern Norway, 3603 Kongsberg, Norway

Corresponding author: Hieu T. Nguyen (hieu.nguyen@usn.no)

The work of Hung N. Dang was supported in part by Vingroup Joint Stock Company, and in part by the Domestic Ph.D. Scholarship Program of Vingroup Innovation Foundation (VINIF), Vingroup Big Data Institute (VINBIGDATA), under Grant VINIF.2020.TS.130.

**ABSTRACT** Nowadays, large-scale multiple-input multiple-output (LS-MIMO) with low-resolution analog-to-digital converters (ADCs) is a favorable transmission scheme for 5G and beyond wireless networks to reduce the power consumption of the radio frequency chains and to increase the network capacity. This paper derives the joint message-passing detection and decoding algorithm based on the double-layer graph for LS-MIMO communication systems with mixed-ADCs. The new protograph extrinsic information chart (PEXIT) algorithm is developed to analytically evaluate the performance of protograph low-density parity-check code under various mixed-ADC combinations and LS-MIMO configuration scenarios. The simulation results validate the accuracy of the proposed algorithm. Furthermore, our experiments show that the mixed-ADC system can achieve a significant power gain even when only one received antenna is equipped with high-resolution ADCs. It is observed that 4-bit or 5-bit resolution is an optimal choice for the high-resolution receive antennas. Interestingly, mixed-ADC systems with Ternary-ADCs generally provide significant gains at the cost of the increase in the average resolution by a fraction of a bit. There are specific scenarios where the Ternary-ADC-based system outperforms the 1-bit-ADC based system at the same or lower average resolution. In the particular case of  $16 \times 16$  MIMO configuration where the number of low-resolution antennas is  $N_L = 12$  and the number of high-resolution antennas is  $N_H = 4$ , the Ternary-ADC based system can obtain a power gain of about 2 dB at the frame error rate (FER) or bit error rate (BER) level of  $10^{-5}$ .

**INDEX TERMS** Large-scale MIMO, protograph LDPC, low-resolution ADCs, ternary-ADCs, uniform scalar quantizer, truncation limit, mixed-ADCs.

## I. INTRODUCTION

Large-scale multiple-input and multiple-output (LS-MIMO) becomes promising transmission techniques for 5G and future wireless networks to meet the increasing demand for high-speed wireless connections in many practical applications [1], [2], [3]. Nevertheless, a radical challenge for LS-MIMO communication systems with hundreds or thousands of receive antennas is considerably high power consumption imposed by the huge number of radio frequency (RF) chains [4], [5]. For example, mmWave massive MIMO of 256 RF chains equipped with 512 high-resolution

ADCs (8 - 12 bits) have total power consumption as high as 256 Watt [5]. This is because the hardware cost and the power consumption of ADCs and DACs linearly increase with the bandwidth and exponentially with the number of bits used in the ADCs. To cope with that difficulty, an encouraging solution is to replace the power-hungry high-resolution ADCs with low-power low-resolution ADCs [5]–[14]. Opting for low-resolution ADCs can lead to a performance loss of the baseband signal processing blocks, such as channel gain estimation and signal detection.

This paper investigates a joint detection and protograph LDPC coding algorithm based on a double-layer graph for massive MIMO communication systems where mixed-ADCs are employed to reduce power consumption.

The associate editor coordinating the review of this manuscript and approving it for publication was Jinming Wen.

Furthermore, the analytical tool is developed to evaluate the system performance when the ratio between the number of low-resolution antennas and the number of high-resolution antennas, so-called the antenna partition ratio, varies.

### A. RELATED WORKS

There has been an extensive amount of research work to deal with the effect of low resolution and hardware impairment on the system performance [9], [11]–[14]. Nguyen *et al.* proposed learning techniques - utilizing the redundancy check or to-be-decoded data to assist the learning process - to cope with the circumstances where the channel state information (CSI) is imperfect or unavailable at the BS. The learning method yields performance enhancement and robustness to the massive MIMO with low-resolution ADCs [10]. Adopting a similar method, Gao *et al.* [9], employed deep learning techniques to resolve channel estimation issues, but for massive MIMO with the mixed ADCs (i.e., *the system where a small portion of antennas has high-resolution ADCs while the rest has low-resolution ADCs*). In this work, the approach to reduce the adverse impact of the low-resolution ADCs is to use the signals received by the high-resolution ADC antennas to predict the channels of other antennas and their channels. This strategy achieves performance improvement for the case of 1-bit mixed ADCs.

For signal detection algorithms in LS-MIMO communication systems with low-resolution ADCs, authors in [14] investigated the two-stage signal detector based on the zero-forcing (ZF) and maximum likelihood (ML) detector for the LS-MIMO systems with 1-bit ADCs. This proposed detector performs better than the conventional ZF detector, while its complexity is much lower than the ML detector. Dealing with 1-bit ADC MIMO systems where message-passing channel decoder is used, Cho and Hong [13] derived an algorithm to calculate the soft metric (e.g., a log-likelihood ratio) for the MIMO signal detector. This approach's advantage is that the MIMO detector and the message-passing channel decoder can exchange the log-likelihood ratio of the coded bit with each other, and the inter-stream interference is also canceled. As a result, this soft-output detector outperforms the ZF-type detector in perfect and imperfect CSI cases at the basestation. In the same line of the soft-output MIMO detector, Nguyen *et al.* [12], investigated the coded massive MIMO systems where few-bit ADCs and protograph low-density parity-check (LDPC) codes were applied. The joint MIMO detection and decoding with parallel interference cancellation algorithm was used at the receiver. The study indicated that a large number of antennas at the receiver could compensate for the low-resolution of the ADCs. The 4-bit ADC systems' performance could approach the performance of the high-resolution systems under various LS-MIMO configurations.

Concerning the theoretical performance (i.e., the achievable sum-rate) of MU-MIMO systems with low-resolution ADCs, Fan *et al.* [4], derived the approximation sum-rate expression for single-cell MU-MIMO systems in which both

large-scale fading and fast fading effects are taken into account. Similar to findings in [11], Fan *et al.* indicated that the performance loss could be compensated by increasing the number of receiving antennas. Furthermore, the energy efficiency, which is accounted for both transmit power over the channel and the power dissipation of the ADCs at the antennas [15], was investigated, and it was shown that 1-bit or 2-bit ADCs achieved the best energy efficiency. Recently, Dang *et al.* [16], derived the formula to calculate the truncation limits of the low-resolution ADCs to improve the achievable uplink MU-MIMO communication systems.

The impact of the signal detection on the energy efficiency was also investigated by Lui *et al.* [7]. In this work, the authors focused on investigating the ZF detector's performance and its variant, ZF successive interference cancellation (ZF-SIC). The power allocation strategy was derived in analytical form by considering the equal transmission rate for all users. Additionally, Dai *et al.* studied the achievable rate for both uplink and downlink of full-duplex massive MIMO systems with low-resolution ADCs [8]. The results revealed that using proper power scaling law and more antennas at the BS could reduce the interference and noise. Furthermore, it is again proven that increasing the resolution of ADCs is not the right choice since the system performance is limitedly improved while the overhead and power consumption unreasonably increase. Ultimately, the study suggested that low-resolution ADCs are a practical option for massive MIMO systems.

The previous studies on mixed-ADC LS-MIMO systems mainly relied on information theory where a random code with infinite code length was assumed. Little attention was paid to pragmatic communication systems where a specific family of channel correcting codes should be employed. The closely related study of protograph LDPC codes' performance in low-resolution ADC LS-MIMO communication systems was carried by Nguyen *et al.* [12]. Nevertheless, this study was only for all-low-resolution ADCs. Hence, the research in this paper is going to explore the performance of mixed-ADC LS-MIMO communication systems where the capacity-approaching and low-complexity protograph LDPC codes are used as in the channel coding block.

### B. CONTRIBUTIONS

This study aims to evaluate the performance of mixed-ADCs in LS-MIMO protograph LDPC coded communication systems. The main contributions are summarized as follows:

- Design the joint signal detection and channel decoding based on a double-layer graph. On this graph, the MIMO layer is divided into two sub-graphs - one for low-resolution ADC observation nodes and one for high-resolution ADC observation nodes. The mathematic expressions of the extrinsic information are derived to show the role of high-resolution antennas in helping improve the system performance.
- Design the protograph extrinsic information chart algorithm for large-scale MIMO channels with

mixed-ADCs, so-called Mixed-ADC-LS-MIMO-PEXIT. The algorithm is a powerful tool to obtain theoretical/analytical performance metrics of any family of the protograph LDPC codes - the iterative decoding threshold.

- Propose to use Ternary-ADCs (ADCs with only three quantization levels) in the low-resolution antennas. Both analytical and simulation results prove that the use of Ternary-ADCs as low-resolution ADCs in the mixed-ADC systems can dramatically improve the performance as much as about 2 dB while the average resolution is kept at the same or lower level than that of the other mixed-ADC system. Experiments are also carried out to find the best resolution combination. When using Ternary-ADC at low-resolution antennas in the mixed-ADC system, the best resolution of the high-resolution antennas is either 4 or 5 bits.

### C. OUTLINE

The remaining of this paper is organized as follows: Section II describes protograph LDPC coded communication systems where mixed-ADC LS-MIMO transmission scheme is employed. The joint LS-MIMO signal detection and channel decoding algorithm based on the double-layer graph is presented in Section III. Section IV design the Mixed-ADC-LS-MIMO-PEXIT algorithm, which is used as a powerful tool to analyze the performance metric of protograph LDPC codes in LS-MIMO communication systems with mixed-ADCs in Section V. The simulations are carried out in Section VI to validate the analytical results obtained from the proposed PEXIT algorithm. Section VII concludes the paper.

*Notation:* Lowercase and uppercase boldface letters are used to denote vectors and matrices, respectively, while the lightface letters denote scalars. Besides, an identity matrix with an appropriate dimension is denoted as  $\mathbf{I}$ .  $\text{diag}(\mathbf{A})$  represents the main diagonal of  $\mathbf{A}$ .  $(\cdot)^T$  denotes the transpose of a matrix or vector, and  $(\cdot)^*$  denotes the corresponding complex number.  $I[\cdot, \cdot]$  is the mutual information between two random variables.  $\mathcal{N}(a, b)$  and  $\mathcal{CN}(a, b)$  denote real and complex Gaussian distributed variable with mean  $a$  and covariance  $b$ .  $\Phi(\cdot)$  denotes the quantization operation.  $J(\cdot)$  denotes the approximate calculation of mutual information. Finally, the subscripts ‘‘H’’ and ‘‘L’’ denote the high-resolution and low-resolution antenna groups, respectively.

## II. SYSTEM MODEL

Consider a wireless fading multiple-input-multiple-output (MIMO) channel with  $M$  transmitting and  $N$  receiving antennas with  $2N$  pairs of mixed-ADCs, as shown in Fig. 1. A block of  $K_c$  information bits is first encoded by a P-LPDC encoder that produces a codeword with a length of  $N_c$  coded bits. The coded bits  $c \in \{0, 1\}$  are passed to a binary-phase-shift-keying (BPSK) modulator whose output is given by  $s = (-1)^c \in \{+1, -1\}$ . In one channel use, using the spatial multiplexing scheme [20],  $M$  modulated symbols are transmitted over  $M$  transmitting antennas. It thus requires  $L = \lceil N_c/M \rceil$  channel uses to transfer all  $N_c$  coded bits.

The received signal model is given by

$$\mathbf{r} = \mathbf{H}\mathbf{x} + \mathbf{w}. \quad (1)$$

Here,  $\mathbf{x} = [x[1], x[2], \dots, x[M]]^T$  is the vector of the transmitted symbol whose elements belong to the BPSK modulation alphabet. The average symbol energy  $E_s = \mathbb{E}(\|\mathbf{x}\|^2)$  is normalized to 1.  $\mathbf{H} \in \mathbb{C}^{N \times M}$  is channel matrix whose entries  $h[n, m]$  in the  $n$ -th row and  $m$ -th column of  $\mathbf{H}$  are modeled as i.i.d complex Gaussian with zero mean and unit variance  $\mathcal{CN}(0, 1)$ . In this work, the perfect channel state information (CSI) is assumed to be available at the receiver, but not at the transmitter. The vector  $\mathbf{w} = [w[1], w[2], \dots, w[N]]^T \in \mathbb{C}^{N \times 1}$  is complex additive white Gaussian noise vector whose entries obey i.i.d complex Gaussian with zero mean and  $N_0$  variance (i.e.,  $\mathcal{CN}(0, N_0)$ ). Finally,  $\mathbf{r} = [r[1], r[2], \dots, r[N]]^T \in \mathbb{C}^{N \times 1}$  is the received signal vector whose element  $r[n]$  is the received signal at the  $n$ -th antenna.

The received signal vector  $\mathbf{r}$  consists of two sub-vectors  $\mathbf{r}_L$  with a length of  $N_L$  and  $\mathbf{r}_H$  with a length of  $N_H = N - N_L$ , which are received signals at the input of the low-resolution and high-resolution antenna groups, respectively. We can break down the received signal vector  $\mathbf{r}$  into those two sub-vectors as follows:

$$\mathbf{r}_\zeta = \mathbf{H}_\zeta \mathbf{x} + \mathbf{w}_\zeta, \quad \zeta \in \{L, H\}, \quad (2)$$

where  $\mathbf{H}_\zeta \in \mathbb{C}^{N_\zeta \times M}$  and  $\mathbf{w}_\zeta \in \mathbb{C}^{N_\zeta \times 1}$ .

The received signal sub-vector  $\mathbf{r}_L$  is fed to  $2N_L$  pairs of low-resolution ADCs (i.e., 1-bit ADCs or Ternary-ADCs in this paper). While the other sub-vector  $\mathbf{r}_H$  is applied to  $2N_H$  pairs of high-resolution ADCs limited to 3-bit to 5-bit ADCs in this paper since it has been proven that 5-bit ADC system approaches the full-resolution system [12]. It is worth noting that in many previous research works on the mixed-ADC LS-MIMO systems, the resolution level of the high-resolution antenna group is from 8 - 10 bits/sample. In contrast, it is proven by both the theory and simulation results in this paper that 4 or 5 bits are good resolution levels for the high-resolution antenna group.

Let  $\Phi$  be the quantization function, the relations between the input and output of the  $Q_\zeta$ -bit ADC is given by

$$\mathbf{y}_\zeta = \Phi(\mathbf{r}_{\zeta, re}) + j\Phi(\mathbf{r}_{\zeta, im}), \quad (3)$$

where  $\zeta \in \{L, H\}$ , and  $\mathbf{r}_{\zeta, re}$  and  $\mathbf{r}_{\zeta, im}$  are the real and imaginary components of the received signal  $\mathbf{r}_\zeta$ , respectively. Furthermore, the quantizer function  $\Phi$  in this paper is the scalar one (i.e., each element in the vector is quantized separately).

Adopting the additive quantization noise model (AQNМ), which is often employed in MIMO systems with low-resolution ADCs [4], [21], we consider the quantization noise as the additive noise component to the input signal. According to the AQNM model, the relationship between the input and output of the quantizer in (3) can be mathematically written as below [4]:

$$\mathbf{y}_\zeta = \varphi_\zeta \mathbf{r}_\zeta + \mathbf{w}_{\zeta, \Phi}, \quad \zeta \in \{L, H\}, \quad (4)$$

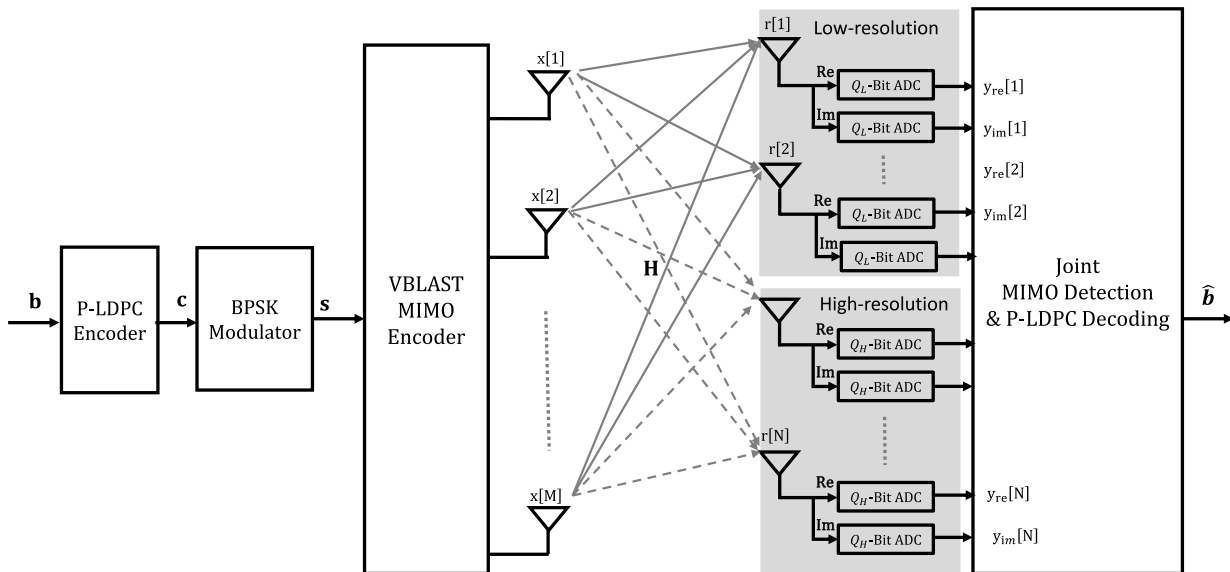


FIGURE 1. The channel model of the LS-MIMO coded communication system with mixed-ADCs.

where  $\varphi_\zeta = 1 - \rho_\zeta$  and  $\rho_\zeta$  is the inverse of the signal-to-quantization-noise ratio of the  $Q_\zeta$ -bit ADCs.  $\mathbf{w}_{\zeta, \Phi}$ ,  $\zeta \in \{L, H\}$  is the additive Gaussian noise vector that is assumed uncorrelated with  $\mathbf{r}_\zeta$ .

For a given channel realization matrices  $\mathbf{H}_\zeta$ ,  $\zeta \in \{L, H\}$ , the variance of  $w_{\zeta, \Phi}[n_\zeta]$ ,  $n_\zeta = 1, 2, \dots, N_\zeta$  is given by [4]

$$\sigma_\zeta^2[n_\zeta] = \varphi_\zeta(1 - \varphi_\zeta) \left( \sum_{m=1}^M |h_\zeta[n_\zeta, m]|^2 + N_0 \right), \quad (5)$$

where  $h_\zeta[n_\zeta, m]$  is the element of matrix  $\mathbf{H}_\zeta$ . Note that the variances depend on the fading channel gains  $h_\zeta[n_\zeta, m]$  and the additive Gaussian noise at the receiver antenna,  $N_0$ , which is again the variance of the additive Gaussian noise in (1).

In this research work, uniform quantizers, [22], are employed, but the following analysis can be also applicable to non-uniform ones. With the assumption of the channel model in (1), the input signals of the  $Q_L$ -bit and  $Q_H$ -bit ADCs in Fig. 1 are continuous random variables with infinite supports. Therefore, the input signals,  $r_\zeta[n_\zeta]$ ,  $n_\zeta = 1, 2, \dots, N_\zeta$ ,  $\zeta \in \{L, H\}$ , are first truncated to obtain the finite supports in the range  $[-T_{\zeta, s}, T_{\zeta, s}]$ . The truncation process is mathematically expressed as below:

$$\overline{r_\zeta[n_\zeta]} = \begin{cases} -T_{\zeta, s}, & r_\zeta[n_\zeta] < -T_{\zeta, s}; \\ r_\zeta[n_\zeta], & -T_{\zeta, s} \leq r_\zeta[n_\zeta] \leq T_{\zeta, s}; \\ T_{\zeta, s}, & r_\zeta[n_\zeta] > T_{\zeta, s}. \end{cases} \quad (6)$$

where  $\overline{r_\zeta[n_\zeta]}$  is the truncated version of the received signal -  $r_\zeta[n_\zeta]$ . The optimal value of  $T_{\zeta, s}$ ,  $\zeta \in \{L, H\}$  depends on the probability density distribution of the input signal and the number of quantization levels [23]. In [16], Dang et al. derived the formula to calculate the optimal truncation limits and the performance metric  $\varphi_\zeta$  for different resolution levels which are listed in Table 1.

TABLE 1. Truncation limit and performance merit of low-resolution ADCs.

	1-ADC	Ternary-ADC	2-ADC	3-ADC	4-ADC	5-ADC
$T_s$	1.699	1.922	2.091	2.461	2.791	3.028
$\varphi$	0.6261	0.8095	0.8796	0.9628	0.9885	0.9963

Note that the parameters  $\varphi_\zeta$ ,  $\zeta \in \{L, H\}$  depends on the resolution of the ADCs and the truncation limit. It is observed that the lower the resolution, the smaller the truncation limit, as shown in Table 1. It is worth noting that the 3 -  $\sigma$  rule truncation limit, which has often been used in quantized LS-MIMO communication systems [12], is optimal only for the resolution more than or equal 5 bits [16].

### III. JOINT DETECTION AND DECODING RECEIVER FOR LOW-RESOLUTION MIXED-ADC LS-MIMO SYSTEMS

When the number of antennas is in order of tens or hundreds, the conventional MIMO detection algorithms such as zero-forcing, minimum mean square error spatial filtering, sphere decoding, and maximum likelihood detector are computationally prohibitive [24], [25]. The maximum ratio combining (MRC) signal detection is widely employed in the research work on the topic of low-resolution ADC LS-MIMO transmission [11]. This detection scheme offers low system performance due to the inter-stream inference. Recently, the message-passing algorithm is an attractive solution to deal with the complexity issue and to improve the system performance by canceling the inter-stream interference via iterative joint detection and decoding [12]. Nevertheless, this message-passing algorithm was derived for LS-MIMO systems where the whole receiving antenna group is equipped with the same type of low-resolution ADCs. Hence, in this section, we derive the joint detection and decoding algorithm on the double-layer graph where there are two types of

observation nodes - the low-resolution and high-resolution observation nodes as shown in Fig. 2.

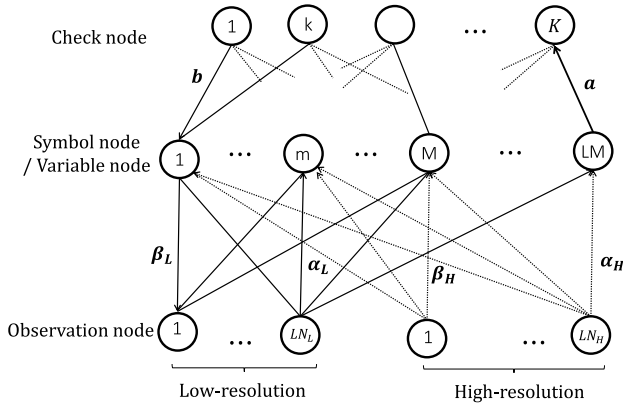


**FIGURE 2.** Double-layer graph for joint detection and decoding receiver with mixed-ADCs.

We employ the double-layer graph in Fig. 2 to provide a clear description of the joint detection and decoding algorithm. The double-layer graph has three types of nodes, namely: 1)  $L \times N$  observation nodes representing the received signal sequence  $\mathbf{r}$ . The set of observation nodes is divided into two subsets - one subset for the  $N_L$  low-resolution received antennas and one set for the  $N_H$  high-resolution received antennas. Note that  $N = N_L + N_H$ ; 2)  $N_c = L \times M$  symbol nodes that represent the transmit symbol sequence  $\mathbf{x}$ ; 3) Finally, there are  $K = N_c - K_c$  check nodes that represent the check equations of given P-LDPC codes. The connections of the variable node and the check node are governed by the parity matrix of the LDPC code. In one channel use, the  $N$  observation nodes and the  $M$  symbol nodes are fully connected to form a graph for the MIMO detection part (i.e., one observation node is connected to all  $M$  symbol nodes). In the graph for the LDPC decoding part, there are  $N_c$  variable nodes that represent the codeword bit sequence  $\mathbf{c}$ . With the BPSK modulation scheme, the one-one mapping is used to map a codeword bit to a transmit symbol. Therefore, the variable node and the symbol node are merged in a single node on the double-layer graph. Consequently, the two terms - the variable node and symbol node - are used interchangeably in this paper.

In the iterative joint detection and decoding algorithm, there are seven types of messages passed over the graph as follows:

- $\alpha_L[n_L, m]$  is the message passed from the  $n_L$ -th low-resolution observation node to the  $m$ -th symbol node.
- $\alpha_H[n_H, m]$  is the message passed from the  $n_H$ -th high-resolution observation node to the  $m$ -th symbol node.
- $a[m, k]$  is the message passed from the  $m$ -th variable node to the  $k$ -th check node.
- $b[k, m]$  is the message passed from the  $k$ -th check node to the  $m$ -th variable node.

- $\beta_L[m, n_L]$  is the message passing from the  $m$ -th symbol node to the  $n_L$ -th low-resolution observation node.
- $\beta_H[m, n_H]$  is the message passing from the  $m$ -th symbol node to the  $n_H$ -th high-resolution observation node.
- $\Gamma[m]$  is the a posteriori log-likelihood ratio (LLR) value of the symbol  $x[m]$ .

Those messages flow back and forth on the double-layer and the detailed expressions to calculate them are presented in the following subsections.

### A. MESSAGE PASSED FROM OBSERVATION NODES TO SYMBOL NODES

The received signal at the  $n_\zeta$ -th observation node,  $n_\zeta = 1, 2, \dots, N_\zeta$ ,  $\zeta \in \{L, H\}$ , is given as

$$\begin{aligned} y_\zeta[n_\zeta, m] &= \varphi_\zeta r_\zeta[n_\zeta] + w_{\zeta, \Phi}[n_\zeta] \\ &= \varphi_\zeta \sum_{m=1}^M h_\zeta[n_\zeta, m] x[m] + \varphi_\zeta w[n_\zeta] + w_{\zeta, \Phi}[n_\zeta] \\ &= \varphi_\zeta h_\zeta[n_\zeta, m] x[m] + \varphi_\zeta \underbrace{\sum_{t=1, t \neq m}^M h_\zeta[n_\zeta, t] x[t]}_{\text{Interference}} \\ &\quad + \varphi_\zeta w[n_\zeta] + w_{\zeta, \Phi}[n_\zeta]. \end{aligned} \quad (7)$$

In comparison with unquantized LS-MIMO systems (or high-resolution systems), the received signals at the  $n_L$ -th low-resolution antenna and the  $n_H$  high-resolution antenna for the symbol  $x[m]$  have extra noise components (quantization noise components which are depending on the resolution and truncation limit of the ADCs). Their signal strength levels are affected by the quantization process via the parameters  $\varphi_L$  and  $\varphi_H$ .

In this work, the parallel interference cancellation technique [25] is exploited to reduce the effect of the inter-substream interference components in (7). The soft symbols are first estimated based on the extrinsic message passed from the  $m$ -th symbol node to the  $n_L$ -th observation node and the  $n_H$ -th observation node. Let  $\hat{x}[n_L, m]$  and  $\hat{x}[n_H, m]$  denote the soft symbols obtained from the messages passed from the  $n_L$ -th low-resolution observation node and the  $n_H$ -th high-resolution node to the  $m$ -th symbol node. For the BPSK modulation scheme, the soft symbol is given by

$$\hat{x}[n_\zeta, m] = \tanh\left(\frac{\beta_\zeta[m, n_\zeta]}{2}\right), \quad \zeta \in \{L, H\}, \quad (8)$$

where  $\beta_\zeta[m, n_\zeta]$  is the extrinsic message passed from the  $m$ -th symbol node to the  $n_\zeta$ -th observation node. We assume that  $\beta_\zeta[m, n_\zeta], \forall n_\zeta = 1, 2, \dots, LN_\zeta, \forall m = 1, 2, \dots, LM$  are uncorrelated and satisfy the consistency condition [26]. The soft symbols in (8) are now employed to eliminate the effect of the inter-stream interference from the received signal at the  $n_\zeta$ -th observation node for the  $m$ -th transmit symbol,  $x[m]$ , as below

$$\hat{y}_\zeta[n_\zeta, m] = y_\zeta[n_\zeta, m] - \varphi_\zeta \sum_{t=1, t \neq m}^M h_\zeta[n_\zeta, t] \hat{x}[n_\zeta, t], \quad (9)$$

where  $\hat{y}_\zeta[n_\zeta, m]$  is the received signal of the transmitted symbol  $x[m]$  at the  $n_\zeta$ -th observation node after the interference cancellation.

Technically, the soft symbol  $\hat{x}[n_\zeta, m]$  is an imperfect replica of the transmitted symbol  $x[m]$ . Hence, the residual interference components remain in the signal  $\hat{y}_\zeta[n_\zeta, m]$  after cancellation process in (9). Let  $z_\zeta[n_\zeta, m]$  be the residual interference plus noise components of the received signal. We have

$$z_\zeta[n_\zeta, m] = \varphi_\zeta \sum_{t=1, t \neq m}^M h_\zeta[n_\zeta, t](x[n_\zeta, t] - \hat{x}[n_\zeta, t]) + \varphi_\zeta w[n_\zeta] + w_{\zeta, \Phi}[n_\zeta], \zeta \in \{L, H\}. \quad (10)$$

We can now rewrite  $\hat{y}_\zeta[n_\zeta, m]$ ,  $\zeta \in \{L, H\}$  as below

$$\hat{y}_\zeta[n_\zeta, m] = \varphi_\zeta h_\zeta[n_\zeta, m]x[m] + z_\zeta[n_\zeta, m] \quad (11)$$

By approximating the residual interference components as additive Gaussian noise, the variance of the residual interference plus noise component,  $z_\zeta[n_\zeta, m]$ ,  $\zeta \in \{L, H\}$ , is calculated as

$$\begin{aligned} \Psi_\zeta[n_\zeta, m] &= \varphi_\zeta^2 \sum_{t=1, t \neq m}^M |h_\zeta[n_\zeta, t]|^2 (1 - |\hat{x}[n_\zeta, t]|^2) \\ &\quad + \varphi_\zeta^2 N_0 + \varphi_\zeta (1 - \varphi_\zeta) \left( \sum_{m=1}^M |h_\zeta[n_\zeta, m]|^2 + N_0 \right), \end{aligned} \quad (12)$$

The message passed from the  $n_\zeta$ -th observation node to the  $m$ -th variable node is the log-likelihood ratio (LLR) and given by

$$\begin{aligned} \alpha_\zeta[n_\zeta, m] &= \ln \frac{\Pr(\hat{y}_\zeta[n_\zeta, m] | \mathbf{H}_\zeta, x[m] = +1)}{\Pr(\hat{y}_\zeta[n_\zeta, m] | \mathbf{H}_\zeta, x[m] = -1)} \\ &= \frac{4\varphi_\zeta}{\Psi_\zeta[n_\zeta, m]} \mathfrak{R}(h_\zeta^*[n_\zeta, m] \hat{y}_\zeta[n_\zeta, m]), \zeta \in \{L, H\}. \end{aligned} \quad (13)$$

### B. MESSAGE PASSED FROM VARIABLE NODES TO CHECK NODES

Considering the  $m$ -th variable node, two types of messages are sent to this node. The first type of messages is from the  $LN = LN_L + LN_H$  observation nodes belonging to the part of the MIMO detection graph, and the other type of messages is from the check nodes belonging to the part of the LDPC decoding graph. As a result, the extrinsic message from the  $m$ -th variable node to the  $k$ -th check node is the sum of all the messages from the observation nodes and the check nodes except the message from the  $k$ -th check node. We have

$$a[m, k] = \sum_{\zeta \in \{L, H\}} \sum_{t \in \mathcal{N}_{\zeta, o}(m)} \alpha_\zeta[t, m] + \sum_{t \in \mathcal{N}_c(m) \setminus k} b[t, m], \quad (14)$$

where  $\mathcal{N}_c(m)$  is the set of check nodes connected to the  $m$ -th variable node, and  $\mathcal{N}_{L, o}(m)$  and  $\mathcal{N}_{H, o}(m)$  are the sets of low-resolution and high-resolution observation nodes connected to the  $m$ -th variable node, respectively. In comparison with the algorithm in [12], the extrinsic information from the variable nodes to the check nodes consists of extrinsic information components from the low-resolution and high-resolution observation nodes. The higher level of reliability provided by the high-resolution observation nodes not only helps improve the performance of the signal detection part but also improve the performance of the decoding part thanks to the joint detection and decoding structure of the receiver.

### C. MESSAGE PASSED FROM CHECK NODES TO VARIABLE NODES

The message from the  $k$ -th check node to the  $m$ -th variable node is identical to the conventional message-passing algorithm [27] and given by

$$b[k, m] = \ln \frac{1 - \prod_{t \in \mathcal{N}_v(k) \setminus m} \frac{1 - e^{a[t, k]}}{1 + e^{a[t, k]}}}{1 + \prod_{t \in \mathcal{N}_v(k) \setminus m} \frac{1 - e^{a[t, k]}}{1 + e^{a[t, k]}}}, \quad (15)$$

where  $\mathcal{N}_v(k)$  is the set of variable nodes connected to the  $k$ -th check node. In practical implementation, the computation of  $b[k, m]$  is simplified by using the  $\tanh(\cdot)$  function.

### D. MESSAGE PASSED FROM SYMBOL NODES TO OBSERVATION NODES

The  $m$ -th symbol node receives messages from the  $N_L$  low-resolution observation nodes, the  $N_H$  high-resolution observation nodes, and the check nodes. The extrinsic message sent from the  $m$ -th symbol node to the  $n_L$ -th observation node is the sum of all the messages except the itself message from the  $n_L$ -th low-resolution observation node. As a result, the message from the  $m$ -th variable node to the  $n_L$ -th observation node is given by

$$\begin{aligned} \beta_L[m, n_L] &= \sum_{t \in \mathcal{N}_{L, o}(m) \setminus n_L} \alpha_L[t, m] \\ &\quad + \sum_{t \in \mathcal{N}_{H, o}(m)} \alpha_H[t, m] \\ &\quad + \sum_{t \in \mathcal{N}_c(m)} b[t, m], \text{ for } n_L = 1, 2, \dots, N_L, \end{aligned} \quad (16)$$

where  $\mathcal{N}_{L, o}(m)$ ,  $\mathcal{N}_{H, o}(m)$ , and  $\mathcal{N}_c(m)$  are the sets of the low-resolution observation nodes, the high-resolution observation nodes, and check nodes that are connected to the  $m$ -th symbol node, respectively.

Similarly, the extrinsic message sent from the  $m$ -th symbol node to the  $n_H$ -th high-resolution observation node is the sum of all the messages except the itself message from the  $n_H$ -th high-resolution observation node. As a result, the message from the  $m$ -th variable node to the  $n_H$ -th observation

node is given by

$$\begin{aligned} \beta_H[m, n_H] &= \sum_{t \in \mathcal{N}_{H,o}(m) \setminus n_H} \alpha_H[t, m] \\ &+ \sum_{t \in \mathcal{N}_{L,o}(m)} \alpha_L[t, m] \\ &+ \sum_{t \in \mathcal{N}_c(m)} b[t, m], \text{ for } n_H = 1, 2, \dots, N_H, \end{aligned} \quad (17)$$

where  $\mathcal{N}_{L,o}(m)$ ,  $\mathcal{N}_{H,o}(m)$ , and  $\mathcal{N}_c(m)$  are the sets of all observation nodes and check nodes that are connected to the  $m$ -th symbol node, respectively.

Observed from (16) and (17) that the higher reliability of the extrinsic message of the high-resolution observation nodes improves the reliability levels of extrinsic messages  $\beta_L[m, n_L]$  of the low-resolution observation nodes thanks to the nature of the message-passing algorithm and the broadcasting nature of the wireless communication systems where the message from one observation node propagates to all symbol nodes and this message is sent back to the other observation nodes in the following iteration.

#### E. A POSTERIORI MESSAGES OF CODEWORD BITS

The posterior LLR of the  $m$ -th transmit symbol at the end of each iteration is the total messages from both the observation nodes and the check nodes, and it is given by

$$\Gamma[m] = \sum_{\zeta \in \{L,H\}} \sum_{n_\zeta \in \mathcal{N}_{\zeta,o}(m)} \alpha_\zeta[n_\zeta, m] + \sum_{k \in \mathcal{N}_c(m)} b[k, m]. \quad (18)$$

The posteriori LLR is sent to the hard decision device to produce the decoded version of the codeword bit using the following rule:

$$\hat{c}[m] = \begin{cases} 0, & \Gamma[m] > 0; \\ 1, & \text{Otherwise.} \end{cases} \quad (19)$$

where  $\hat{c}[m]$  denotes the decoded version of  $c[m]$ . And thus, the decoded sequence of the information  $\hat{\mathbf{b}}$  is obtained.

The message-passing process stops when all check equations are satisfied or the maximum number of iterations is reached. Otherwise, the message-passing process repeats with a message update from the observation nodes in Subsection III-A.

### IV. PROPOSED PEXIT ALGORITHM FOR MIXED-ADC LS-MIMO SYSTEMS

The PEXIT algorithm has been previously developed as a powerful tool to predict the performance of protograph LDPC codes for various channel models [12], [28]–[30]. In [28], the PEXIT algorithm was developed for single-input single-output additive white Gaussian (AWGN) channels. The algorithm was then used to design many effective protograph LDPC codes for AWGN channels [31]. The algorithm was later modified to provide a tool for performance analysis of protograph LDPC codes in fading channels [29].

Vu *et al.* discovered that the two earlier versions of the PEXIT algorithm could not directly apply in the case of LS-MIMO communication systems where the joint signal detection and decoding is used to improve the system performance and a new version of PEXIT, the so-called LS-MIMO-PEXIT algorithm, was developed for LS-MIMO channels. The LS-MIMO-PEXIT algorithm was employed to design new protograph LDPC codes for LS-MIMO channels. Another version of the PEXIT algorithm for LS-MIMO communication systems with low-resolution ADCs was proposed by Nguyen *et al.* in [12]. The proposed PEXIT algorithm was proven to be an effective tool to provide insightful understandings of the effect of the low-resolution on the performance of LS-MIMO communication systems. The version of the PEXIT algorithm in [12] is closely related to the algorithm presented below. Nevertheless, such an algorithm cannot straightforwardly be applied to the scenarios where mixed-ADCs are employed. Hence, the following section presents a new version of the PEXIT algorithm suitable for LS-MIMO communication systems where mixed-ADCs are used at the receiving antennas and the joint detection and decoding architecture is employed.

#### A. JOINT MIMO-LDPC PROTOGRAPH

The mutual information flow of the joint detection and decoding receiver is depicted in Fig. 3 and Fig. 4. This protograph is a down-scaled version of the double-layer graph in Fig. 2. The variable nodes and the symbol nodes are separated into two components to facilitate the information flow analysis below. A forward combiner interconnects them for the forward information flow and a backward combiner for the backward information flow, respectively.

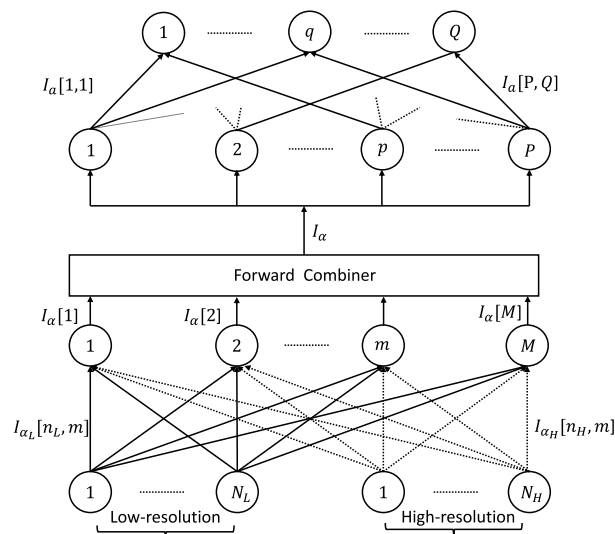


FIGURE 3. Forward information flow.

The MIMO part of the joint MIMO-LDPC protograph consists of  $N_L$  low-resolution observation nodes,  $N_H$  high-resolution observation nodes,  $M$  symbol nodes, and  $M \times N$  edges. This part is duplicated  $L$  times, the

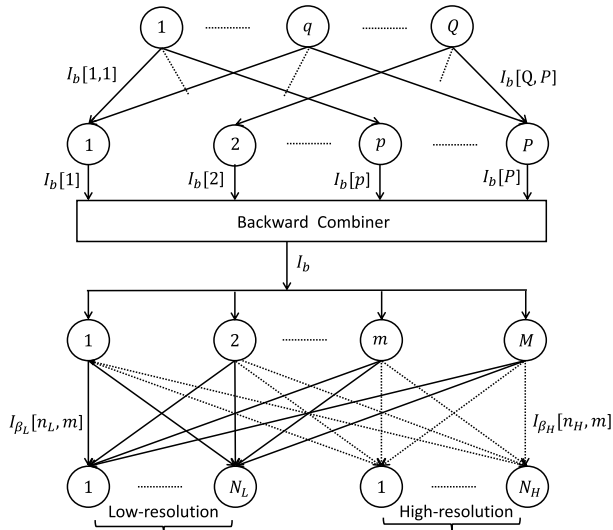


FIGURE 4. Backward information flow.

number of channel uses, to obtain the same MIMO part of the double-layer graph in Fig. 2. On the other hand, the LDPC decoding part of the joint detection and decoding graph has  $P$  variable nodes,  $Q$  check nodes, and a set of edges to connect the variable nodes and check nodes together. The edge connection is defined by a proto-matrix  $\mathbf{B}$  of size  $Q \times P$ . The element  $\mathbf{B}[q, p]$  shows the number of parallel edges that connect the  $q$ -th check node to the  $p$ -th variable node. In order to obtain the LDPC part of the double-layer graph in Fig. 2, the LDPC part of the joint MIMO-LDPC protograph is first copied  $\delta = \frac{N_c}{P} = \frac{LM}{P}$  times and then the permutation operation is applied on  $\delta$  variable-to-check pairs (edges), corresponding to the same edge type of the original protograph [32]. Note that the number of check nodes  $Q = \frac{(N_c - K_c)}{\delta} = (1 - R) \times P$  where  $R$  is the coding rate.

We define seven main types of mutual information, corresponding to the seven extrinsic messages on the double-layer graph in Fig. 2, on the joint MIMO detection and LDPC protograph decoding graph, as follows:

- $I_{\alpha_L}[n_L, m]$  is the extrinsic mutual information between the LLR value  $\alpha_L[n_L, m]$  sent by the  $n_L$ -th low-resolution observation node to the  $m$ -th variable node and the  $m$ -th corresponding coded bit.
- $I_{\alpha_H}[n_H, m]$  is the extrinsic mutual information between the LLR value  $\alpha_H[n_H, m]$  sent by the  $n_H$ -th high-resolution observation node to the  $m$ -th variable node and the  $m$ -th corresponding coded bit.
- $I_a[p, q]$  is the extrinsic mutual information between the LLR value  $a[p, q]$  sent by the  $p$ -th variable node to the  $q$ -th check node and the  $p$ -th corresponding coded bit.
- $I_b[q, p]$  is the extrinsic mutual information between the LLR value  $b[q, p]$  sent by the  $q$ -th check node to the  $p$ -th variable node and the  $p$ -th corresponding coded bit.
- $I_{\beta_L}[m, n_L]$  is the extrinsic mutual information between the LLR value  $\beta_L[m, n_L]$  sent by the  $m$ -th symbol node to the  $n_L$ -th low-resolution observation node and the  $m$ -th corresponding symbol.

- $I_{\beta_H}[m, n_H]$  is the extrinsic mutual information between the LLR value  $\beta_H[m, n_H]$  sent by the  $m$ -th symbol node to the  $n_H$ -th high-resolution observation node and the  $m$ -th corresponding symbol.
- $I_{\Gamma}[p]$  is the posteriori mutual information between the a posteriori LLR value  $\Gamma[p]$  and the corresponding code-word bit of the  $p$ -th variable node.

Besides, we denote the punctured label  $P_p$  of the  $p$ -th variable node as 0 if the  $p$ -th variable node is punctured (i.e., the codeword bits corresponding to this variable node are not transmitted) and 1 otherwise.

### B. FORWARD MUTUAL INFORMATION FLOW

The forward mutual information flow is the direction in which the extrinsic mutual information flows from the observation nodes, goes through the symbol nodes and the variable nodes, and ends at the check nodes as shown in Fig. 3. In the following, the mutual information functions that flow in the forward direction are derived in detail to show the interaction between the low-resolution ADC-graph and the high-resolution-ADC graph.

#### 1) MUTUAL INFORMATION FROM OBSERVATION NODES TO SYMBOL NODES

The  $m$ -th symbol node receives  $N_L$  LLR values sent from all  $N_L$  low-resolution observation nodes and  $N_H$  LLR values sent from  $N_H$  high-resolution observation nodes due to the broadcast nature of the radio signal which is represented by the fully-connected graph in Fig 3. For a fixed channel realization matrix  $\mathbf{H}_\zeta, \zeta \in \{L, H\}$ , the LLR messages transferred from the  $n_\zeta$ -th observation node to the  $m$ -th variable node,  $\alpha_\zeta[n_\zeta, m]$  derived in (13), is given

$$\begin{aligned} \alpha_\zeta[n_\zeta, m] &= \frac{4\varphi_\zeta}{\Psi_\zeta[n_\zeta, m]} \Re(h_\zeta^*[n_\zeta, m] \hat{y}_\zeta[n_\zeta, m]) \\ &= \frac{4}{\Psi_\zeta[n_\zeta, m]} \Re(\varphi_\zeta^2 |h_\zeta[n_\zeta, m]|^2 x[m] + \varphi_{z_\zeta}[n_\zeta, m]) \\ &= \frac{4}{\Psi_\zeta[n_\zeta, m]} (\varphi_\zeta^2 |h_\zeta[n_\zeta, m]|^2 x[m] + \varphi_\zeta \Re(h_\zeta^*[n_\zeta, m] z_\zeta[n_\zeta, m])). \end{aligned}$$

Without loss of generality, we assume that the all-zero codeword is transmitted. And thus, the LLR value  $\alpha_\zeta[n_\zeta, m]$  is given by

$$\alpha_\zeta[n_\zeta, m] = \frac{4}{\Psi_\zeta[n_\zeta, m]} (\varphi_\zeta^2 |h_\zeta[n_\zeta, m]|^2 + \varphi_\zeta \Re(h_\zeta^*[n_\zeta, m] z_\zeta[n_\zeta, m])).$$

Since  $\mathbb{E}[z_\zeta[n_\zeta, m] z_\zeta^*[n_\zeta, m]] = \Psi_\zeta[n_\zeta, m]$  with  $\mathbb{E}(\cdot)$  is expectation operator, we have

$$\begin{aligned} &(\varphi_\zeta^2 |h_\zeta[n_\zeta, m]|^2 + \varphi_\zeta \Re(h_\zeta^*[n_\zeta, m] z_\zeta[n_\zeta, m])) \\ &\sim \mathcal{N}\left(\varphi_\zeta^2 |h_\zeta[n_\zeta, m]|^2, \frac{\varphi_\zeta^2 |h_\zeta[n_\zeta, m]|^2 \Psi_\zeta[n_\zeta, m]}{2}\right). \quad (20) \end{aligned}$$

Consequently, we have

$$\alpha_\zeta[n_\zeta, m] \sim \mathcal{N}\left(\frac{\sigma_{\alpha_\zeta}^2[n_\zeta, m]}{2}, \sigma_{\alpha_\zeta}^2[n_\zeta, m]\right), \quad (21)$$

with

$$\sigma_{\alpha_\zeta}^2[n_\zeta, m] = \frac{8\varphi_\zeta^2|h_\zeta[n_\zeta, m]|^2}{\Psi_\zeta[n_\zeta, m]}. \quad (22)$$

The LLR  $\alpha_\zeta[n_\zeta, m]$  satisfies the symmetric Gaussian distribution for a given channel realization [29]. We achieve the result in (21) with assumption that the interference plus noise components  $z_\zeta[n_\zeta, m]$  is approximated i.i.d complex Gaussian random variable. For the high-resolution case, it was verified by both EXIT chart analysis and simulation result that this assumption is reasonable when the number of receive antenna is large [33].

As a result, the mutual information flows from the  $n_\zeta$ -th observation node to the  $m$ -th symbol node is given by

$$I_{\alpha_\zeta}[n_\zeta, m] = J\left(\sqrt{\frac{8\varphi_\zeta^2|h_\zeta[n_\zeta, m]|^2}{\Psi_\zeta[n_\zeta, m]}}\right), \quad \zeta \in \{L, H\}, \quad (23)$$

where  $J(x)$  function is given in [27].

## 2) MUTUAL INFORMATION FROM SYMBOL NODES TO VARIABLE NODES

The  $m$ -th symbol node receives total  $N = N_L + N_H$  messages from the  $N_L$  low-resolution observation nodes and the  $N_H$  high-resolution nodes, as shown in Fig 3. Let  $\alpha[m]$  be the total message that the  $m$ -th symbol node receives, we have

$$\alpha[m] = \sum_{\zeta \in \{L, H\}} \sum_{n_\zeta}^{N_\zeta} \alpha_\zeta[n_\zeta, m]. \quad (24)$$

According to (21), the total message also follows the Gaussian distribution with mean and variance as follows:

$$\alpha[m] \sim \mathcal{N}\left(\frac{\sigma_\alpha^2[m]}{2}, \sigma_\alpha^2[m]\right), \quad (25)$$

where

$$\begin{aligned} \sigma_\alpha^2[m] &= \sum_{\zeta \in \{L, H\}} \sum_{n_\zeta=1}^{N_\zeta} \sigma_{\alpha_\zeta}^2[n_\zeta, m] \\ &= \sum_{\zeta \in \{L, H\}} \sum_{n_\zeta=1}^{N_\zeta} \frac{8\varphi_\zeta^2|h_\zeta[n_\zeta, m]|^2}{\Psi_\zeta[n_\zeta, m]}, \end{aligned} \quad (26)$$

and thus the extrinsic mutual information,  $I_\alpha[m]$ , is obtained by the following equation

$$I_\alpha[m] = J\left(\sqrt{\sum_{\zeta \in \{L, H\}} \sum_{n_\zeta=1}^{N_\zeta} \frac{8\varphi_\zeta^2|h_\zeta[n_\zeta, m]|^2}{\Psi_\zeta[n_\zeta, m]}}\right). \quad (27)$$

From the expression (27), we can see the influence of the high-resolution ADCs on the total mutual information transferred from the observation nodes to the symbol nodes.

In particular, the high-resolution ADCs has higher value of  $\varphi_H$  and low value of  $\Psi_H[n_H, m]$  which in turn help increase the total variance of  $\sigma_\alpha^2$ . Ultimately, the mutual information transferred from the observation nodes to the symbol nodes is higher than that of the conventional low-resolution ADC systems, where only one type of a low-resolution ADC is employed.

Under the assumption of the infinite code length (i.e.,  $N_c \rightarrow \infty$ ) the code bits belonging to a particular variable node are transmitted by all transmit antennas/symbol nodes with an equal probability of  $1/M$ . Therefore, the functionality of the forward combiner is to calculate the average mutual information from all symbol nodes and then send to the variable nodes. Let  $I_\alpha$  denote the average mutual information from all symbol nodes, we have

$$I_\alpha = \frac{1}{M} \sum_{m=1}^M I_\alpha[m], \quad (28)$$

where  $I_\alpha[m]$  is given in (27). As a result, the channel mutual information flowing from the symbol nodes to the  $p$ -th variable node is given by

$$I_\alpha[p] = P_p I_\alpha, \quad \forall p = 1, 2, \dots, P, \quad (29)$$

where  $P_p = 1$  when node  $p$  is not punctured and  $P_p = 0$  when node  $p$  is punctured.

## 3) MUTUAL INFORMATION FLOW FROM VARIABLE NODES TO CHECK NODES

The expression for the mutual information transferred from the  $p$ -th variable node to the  $q$ -th check node,  $I_a[p, q]$ , is identical to that of the conventional PEXIT algorithm in [28] and given by

$$I_a[p, q] = J\left(\sqrt{[J^{-1}(I_\alpha[p])]^2 + \sigma_b^2[p]}\right), \quad (30)$$

where

$$\sigma_b^2[p] = \sum_{t \in \mathcal{N}_c(p) \setminus k} \mathbf{B}[t, p][J^{-1}(I_b[t, p])]^2,$$

where  $J^{-1}(x)$  is given in [27].

## C. BACKWARD MUTUAL INFORMATION FLOW

The back mutual information flow is the direction in which the extrinsic mutual information flows from the check nodes, goes through the variable and symbol nodes, and ends at the observation nodes as shown in Fig. 4. In what follows, we present the mutual information functions that flow in the backward direction.

### 1) MUTUAL INFORMATION FLOW FROM CHECK NODES TO VARIABLE NODES

The calculation of the mutual information transferred from the  $q$ -th check node to the  $p$ -th variable node is identical to

that of the conventional PEXIT algorithm in [28]. We have  $I_b[q, p]$

$$I_b[q, p] = 1 - J(\sigma_a[q]), \quad (31)$$

where

$$\sigma_a^2[q] = \sum_{t \in \mathcal{N}_v(q) \setminus p} \mathbf{G}[q, t][J^{-1}(1 - I_a[t, q])]^2.$$

### 2) MUTUAL INFORMATION FLOW FROM VARIABLE NODES TO SYMBOL NODES

Let  $I_b[p]$  denote the total mutual information that the  $p$ -th variable node receives from the check nodes. We can express the total mutual information as below

$$I_b[p] = \sum_{q \in \mathcal{N}_c(p)} I_b[q, p]. \quad (32)$$

Under the same assumption of the infinite code length, the probability that a symbol node transmits the codeword bit from the  $p$ -th variable node is  $1/(\sum_{p=1}^P P_p)$ . Therefore, the functionality of the backward combiner is to calculate the average mutual information over all the variable nodes before sending it to the symbol nodes. The average mutual information from the variable nodes to symbol nodes is given by

$$I_b = \frac{\sum_{p=1}^P P_p I_b[p]}{\sum_{p=1}^P P_p}. \quad (33)$$

### 3) MUTUAL INFORMATION FROM SYMBOL NODES TO OBSERVATION NODES

The mutual information transferred from the  $m$ -th symbol node to the  $n_L$ -th low-resolution observation node,  $I_{\beta_L}[m, n_L]$ , is calculated as

$$I_{\beta_L}[m, n_L] = J\left(\sqrt{\sigma_{\alpha_L}^2[m] + \sigma_{\alpha_H}^2[m] + \sigma_b^2}\right), \quad (34)$$

where

$$\begin{aligned} \sigma_b^2 &= [J^{-1}(I_b)]^2 \\ \sigma_{\alpha_L}^2[m] &= \sum_{t \in \mathcal{N}_{L,o(m)} \setminus n_L} [J^{-1}(I_{\alpha_L}[t, m])]^2 \\ &= \sum_{t \in \mathcal{N}_{L,o(m)} \setminus n_L} \sigma_{\alpha_L}^2[t, m] \\ &= \sum_{t \in \mathcal{N}_{L,o(m)} \setminus n_L} \frac{8\varphi_L^2 |h_L[t, m]|^2}{\Psi_L[t, m]}. \end{aligned}$$

The mutual information transferred from the  $m$ -th symbol node to the  $n_H$ -th high-resolution observation node,  $I_{\beta_H}[m, n_H]$ , is calculated as

$$I_{\beta_H}[m, n_H] = J\left(\sqrt{\sigma_{\alpha_H}^2[m] + \sigma_{\alpha_L}^2[m] + \sigma_b^2}\right), \quad (35)$$

where

$$\sigma_{\alpha_H}^2[m] = \sum_{t \in \mathcal{N}_{H,o(m)} \setminus n_H} [J^{-1}(I_{\alpha_H}[t, m])]^2$$

$$\begin{aligned} &= \sum_{t \in \mathcal{N}_{H,o(m)} \setminus n_H} \sigma_{\alpha_H}^2[t, m] \\ &= \sum_{t \in \mathcal{N}_{H,o(m)} \setminus n_H} \frac{8\varphi_H^2 |h_H[t, m]|^2}{\Psi_H[t, m]}. \end{aligned}$$

Expressions in (34) and (35) show clearly the interaction between the low-resolution ADCs and high-resolution ADCs. Thanks to the fully connected graph, the mutual information of the high-resolution nodes flows to the low-resolution observation nodes via the symbol nodes to improve the mutual information levels of the low-resolution nodes and vice versa. This interaction is the cornerstone to improve the performance of mixed-ADC LS-MIMO communication systems. This benefit of the mixed-ADC systems will be verified in the following sections.

### D. THE APP MUTUAL INFORMATION

Calculate  $I_\Gamma[p]$  for the  $p$ -th variable node

$$I_\Gamma[p] = J\left(\sqrt{[J^{-1}(I_a[p])]^2 + \sigma_b^2[p]}\right), \quad (36)$$

where

$$\sigma_b^2[p] = \sum_{t \in \mathcal{N}_c(p)} \mathbf{B}[t, p][J^{-1}(I_b[t, p])]^2.$$

### E. PROPOSED PEXIT ALGORITHM FOR LS-MIMO COMMUNICATION SYSTEMS WITH MIXED-ADCs

The proposed PEXIT algorithm is obtained by applying the mutual information functions in previous subsections with parameters of a given MIMO configuration,  $M \times N$ , and the size of proto-matrix  $\mathbf{B}$ ,  $Q \times P$ , and the channel parameter  $E_b/N_0$ , and the resolution levels of the Mixed-ADCs,  $Q_L$  and  $Q_H$ . The mixed-ADC LS-MIMO-PEXIT algorithm is given below:

#### Step 0: Initialization:

- Select the size of proto-matrix:  $\mathbf{B}$
- Calculate the coding rate:  $R = \frac{P-Q}{\sum_{p=1}^P P_p}$
- Calculate  $N_0 = \frac{M}{R(E_b/N_0)}$
- Obtain the values of  $\varphi_L$  and  $\varphi_H$  from Table 1 accordingly their resolution levels  $Q_L$  and  $Q_H$ , respectively
- Set  $I_{\beta_L} = 0$  and  $I_{\beta_H} = 0$
- Generate  $2F$  LS-MIMO channel realization matrices  $\{\mathbf{H}_{\zeta,1}, \mathbf{H}_{\zeta,2}, \dots, \mathbf{H}_{\zeta,F}\}$ ,  $\zeta \in \{L, H\}$  which follow Rayleigh distribution

#### Step 1: Observation to variable update

- For  $f = 1, 2, \dots, F$ 
  - For  $m = 1, 2, \dots, M$  and  $n_\zeta = 1, 2, \dots, N_\zeta$ ,  $\zeta \in \{L, H\}$ 
    - \* Calculate  $\sigma_{\beta_\zeta} = J^{-1}(I_{\beta_\zeta})$
    - \* Generate  $\beta_{\zeta,f}[m, n_\zeta] \sim \mathcal{N}(\pm \frac{\sigma_{\beta_\zeta}^2}{2}, \sigma_{\beta_\zeta}^2)$
    - \* Estimate soft information  $\hat{x}_f[m, n_\zeta] = \tanh\left(\frac{\beta_{\zeta,f}[m, n_\zeta]}{2}\right)$
    - \* Calculate  $\Psi_{\zeta,f}[n_\zeta, m]$  by using formula (12).

- For  $m = 1, 2, \dots, M$ 
  - \* Calculate  $I_{\alpha,f}[m]$  by using formula (27)
- Calculate the average of  $I_{\alpha,f}$  over all the channel realizations

$$I_{\alpha}[m] = \frac{1}{F} \sum_{f=1}^F I_{\alpha,f}[m], \quad \forall m = 1, 2, \dots, M.$$

- For  $p = 1, 2, \dots, P$ , calculate  $I_{\alpha}[p]$

$$I_{\alpha}[p] = P_p \left( \frac{1}{M} \sum_{m=1}^M I_{\alpha}[m] \right).$$

Note that if the  $p$ -th variable node is punctured, then  $P_p = 0$ . Otherwise,  $P_p = 1$ .

### Step 2: Variable to check update

- For  $p = 1, 2, \dots, P$  and  $q = 1, 2, \dots, Q$ , calculate  $I_a[p, q]$ :
  - if  $\mathbf{B}[p, q] \neq 0$ ,  $I_a[p, q]$  is then calculated by using formula (30)
  - If  $\mathbf{B}[p, q] = 0$ ,  $I_a[p, q] = 0$ .

### Step 3: Check to variable update

- For  $q = 1, 2, \dots, Q$  and  $p = 1, 2, \dots, P$ 
  - if  $\mathbf{B}[q, p] \neq 0$ ,  $I_b[q, p]$  is then calculated by using formula (31)
  - If  $\mathbf{B}[q, p] = 0$ ,  $I_b[q, p] = 0$

### Step 4: Symbol to observation update

- For  $f = 1, 2, \dots, F$ 
  - For  $m = 1, 2, \dots, M$  and  $n_L = 1, 2, \dots, N_L$ ,  $I_{\beta_{L,f}}[m, n_L]$  is then calculated by using (34)
  - For  $m = 1, 2, \dots, M$  and  $n_H = 1, 2, \dots, N_H$ ,  $I_{\beta_{H,f}}[m, n_H]$  is calculated by using formula (35)
- For  $m = 1, 2, \dots, M$  and  $n_L = 1, 2, \dots, N_L$

$$I_{\beta_L}[m, n_L] = \frac{1}{F} \sum_{f=1}^F I_{\beta_{L,f}}[m, n_L]$$

- For  $m = 1, 2, \dots, M$  and  $n_H = 1, 2, \dots, N_H$

$$I_{\beta_H}[m, n_H] = \frac{1}{F} \sum_{f=1}^F I_{\beta_{H,f}}[m, n_H]$$

### Step 5: APP-LLR mutual information calculation

- For  $p = 1, 2, \dots, P$ ,  $I_{\Gamma}[p]$  is then calculated by using formula (36)

**Step 6: Repeat Step 1 - Step 6 until  $I_{\Gamma}[p] = 1$ ,  $\forall p = 1, 2, \dots, P$ .**

The proposed PEXIT algorithm converges when the select  $E_b/N_0$  is above the threshold. Hence, the threshold  $(E_b/N_0)^*$  is the lowest value at which the mutual information between the APP-LLR messages and the corresponding codeword bits converges to 1. As can be seen, the proposed PEXIT algorithm for the mixed-ADCs differs from the one for the low-resolution ADCs [12] in every step, except Step 3. Specifically, the interaction of the low-resolution ADCs and the high-resolution ADCs is taken into account to calculate the mutual information following on the double-layer graph. In the following section, we exploit this proposed

PEXIT algorithm to analyze the performance of the LS-MIMO communication systems with mixed-ADCs and the potential gain of using mixed-ADC systems is thus revealed via the iterative decoding threshold metrics.

## V. ANALYTICAL RESULTS

In this section, we use the proposed Mixed-ADC-LS-MIMO PEXIT in the previous section to calculate the iterative decoding threshold of a specific protograph LDPC code which was designed for the 1-bit ADC LS-MIMO systems [34]. The proto-matrix of the code is given in (37).

$$\mathbf{B}_{1/2} = \begin{pmatrix} 3 & 2 & 0 & 0 & 0 & 1 \\ 2 & 2 & 1 & 1 & 1 & 0 \\ 2 & 1 & 2 & 1 & 1 & 0 \end{pmatrix}_{3 \times 6}. \quad (37)$$

The iterative decoding threshold and the average resolution of the 1-bit ADC system and the mixed-ADC systems of the  $16 \times 16$  MIMO configuration are given in Fig. 5 and Fig. 6. In this experiment, the number of antennas with low-resolution ADCs varies from 8 to 15. Correspondingly, the number of antennas with high-resolution ADCs ranges from 8 to 1. The iterative decoding threshold of the mixed-ADC system where 1-bit ADCs and 5-bit ADCs are combined for the low-resolution and high-resolution antenna groups is the curve with the square marker. The iterative decoding threshold of the mixed-ADC system is lower than that of the 1-bit ADC system with the minimum gap at the point where  $N_L = 15$  and  $N_H = 1$  and the maximum gap at  $N_L = 8$  and  $N_H = 8$ . The minimum gap of 0.55 dB is observed when the number of antennas with 1-bit ADCs is  $N_L = 15$  and the number of antennas with 5-bit ADCs is  $N_H = 1$  or equivalently 6.25% of received antennas equipped with high-resolution ADCs. When increasing the number of high-resolution (5-bit ADCs) antennas to 50%, the iterative decoding threshold gap significantly increases to about 2.843 dB as shown in Table 2. This significant performance improvement is rooted from the fact that the mutual information  $I_{\alpha}$ , in (27), is increased when the number of the high-resolution antennas increases. Nevertheless, the increase of the number of high-resolution antennas should be made with care of the cost of the power consumption.

The similar trend is observed in Fig. 8 for the  $16 \times 32$  MIMO configuration. At the extreme point where the number of antennas with 1-bit ADCs is  $N_L = 31$  and the number of antennas with 5-bit ADCs is  $N_H = 1$  or just 3.125% of the total received antennas equipped with the high-resolution ADCs, the iterative decoding threshold gain is 0.152 dB as shown in Table 3. When increasing the percentage of the high-resolution antennas to 12.5% (i.e.,  $N_L = 28$ ,  $N_H = 4$ ), the gap of 0.562 dB is obtained. Compared with the case of 6.25% of received antennas equipped with the high-resolution ADCs in the  $16 \times 16$  MIMO configuration, the gain of the mixed-ADC  $16 \times 32$  MIMO system decreases.

The other mixed-ADC systems are also considered where Ternary-ADCs are employed at the low-resolution antennas, and 3-bit, 4-bit, or 5-bit ADCs are used at the

TABLE 2. Iterative decoding threshold: 16 × 16 MIMO, code rate R = 1/2.

	$N_L = 15, N_H = 1$	$N_L = 12, N_H = 4$	$N_L = 8, N_H = 8$
1-ADC	5.62	5.62	5.62
Mixed: 1-ADC + 3-ADC	5.131	4.019	2.985
Mixed: 1-ADC + 4-ADC	5.086	3.901	2.823
Mixed: 1-ADC + 5-ADC	5.070	3.866	2.777
Mixed: T-ADC + 3-ADC	2.878	2.569	2.200
Mixed: T-ADC + 4-ADC	2.856	2.496	2.077
Mixed: T-ADC + 5-ADC	2.850	2.474	2.040

TABLE 3. Iterative decoding threshold: 16 × 32 MIMO, code rate R = 1/2.

	$N_L = 31, N_H = 1$	$N_L = 28, N_H = 4$	$N_L = 22, N_H = 10$
1-ADC	0.976	0.976	0.976
Mixed: 1-ADC + 3-ADC	0.841	0.468	-0.159
Mixed: 1-ADC + 4-ADC	0.830	0.429	-0.242
Mixed: 1-ADC + 5-ADC	0.824	0.414	-0.265
Mixed: T-ADC + 3-ADC	-0.775	-0.887	-1.101
Mixed: T-ADC + 4-ADC	-0.781	-0.912	-1.162
Mixed: T-ADC + 5-ADC	-0.783	-0.921	-1.179

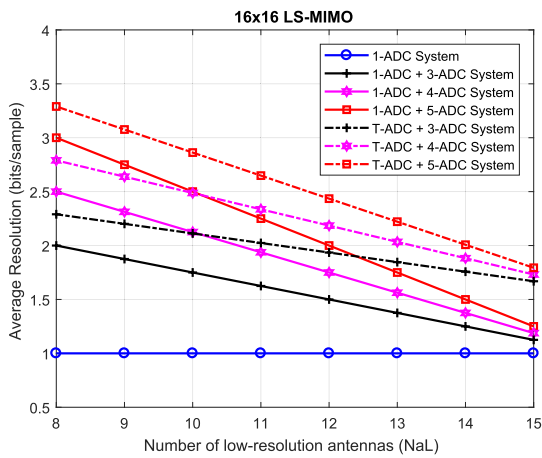


FIGURE 5. Average resolution: 16 × 16 MIMO.

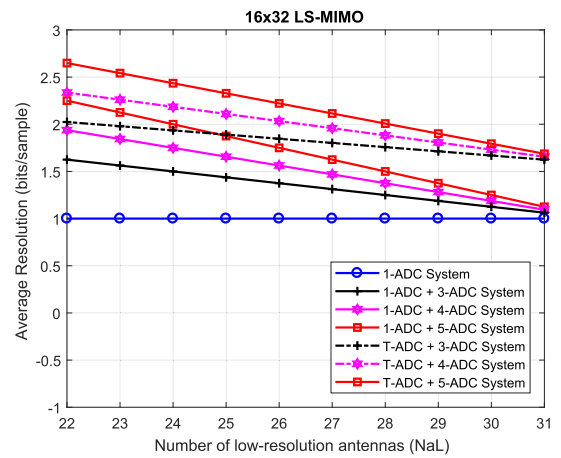


FIGURE 7. Average resolution: 16 × 32 MIMO.

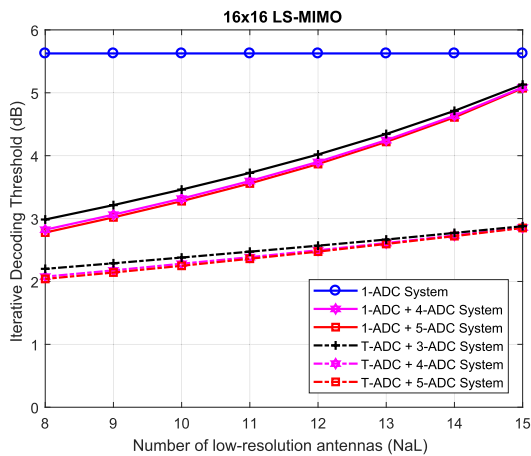


FIGURE 6. Iterative decoding threshold: 16 × 16 MIMO.

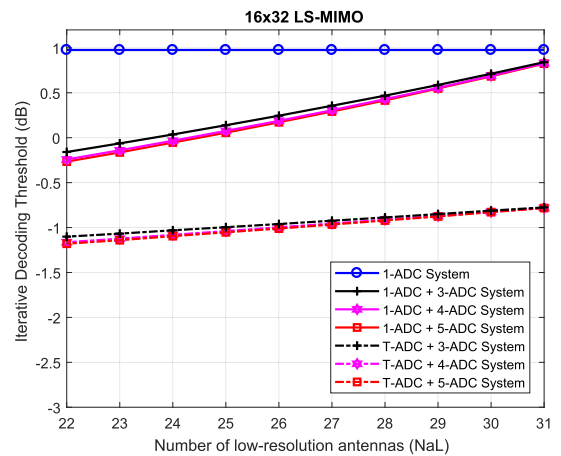


FIGURE 8. Iterative decoding threshold: 16 × 32 MIMO.

high-resolution antennas. The iterative decoding thresholds and average resolution levels are given in Fig. 5 - Fig. 8. The reason for adopting Ternary-ADCs in the LS-MIMO communication systems is that Ternary-ADCs with only

three levels have been proven to be effective to use in many application cases [6]. Observed from Fig. 6 and Fig. 8 that utilizing of Ternary-ADCs for the low-resolution antenna group achieves higher gain than the system with the

combination of 1-bit ADCs and 5-bit ADCs. The highest gain is at the extreme point where the number of high-resolution antennas is at the minimum,  $N_H = 1$ . Specifically, the iterative decoding gaps of the mixed-ADC systems are about 2.77 dB and 1.759 dB for the  $16 \times 16$  MIMO configuration and the  $16 \times 32$  MIMO, respectively. Those gaps translate to additional gains of 2.22 dB and 1.607 dB accordingly by increasing the low-resolution level from one bit to 1.58 bits (Ternary-ADC). The additional gains by using Ternary-ADCs in the low-resolution antenna group can be explained by investigating the argument of  $I_\alpha$  in (27). By using Ternary-ADCs, the better performance merit  $\varphi_L$  is achieved, as shown in Table 1. That makes the argument of  $I_\alpha$  increase and the value of  $I_\alpha$  is, therefore, increased as  $J(\cdot)$  is an increasing function. Put it differently, the reliability of transmitted bit is improved by using Ternary-ADCs in the low-resolution antenna group. As a result, the further performance gains are obtained.

It is observed that 4-bit ADCs seem the best option for the high-resolution antenna group to achieve the lower power consumption of RF chains while a marginal performance loss is seen. The system with the combination of Ternary-ADCs and 5-bit ADCs has a marginal gain compared to the system of the combination of Ternary-ADCs and 4-bit ADCs. The iterative decoding threshold of the combination of Ternary-ADCs and 3-bit ADCs is slightly higher when the number of antennas with high-resolution ADCs increases. In contrast, when the high-resolution antenna portion is small, the gap is negligible, as shown in Fig. 6 and Fig. 8. In particular, when  $N_L = 15$  and  $N_H = 1$ , the iterative decoding threshold of system with the combination of Ternary-ADCs and 3-bit ADCs suffers just 0.028 dB performance loss compared to the system the combination of Ternary-ADCs and 5-bit ADCs for the  $16 \times 16$  MIMO configuration. The gap between the two systems is significantly reduced to 0.008 dB, as shown in Table 3 for the  $16 \times 32$  MIMO configuration.

Looking at Fig. 5, there are some points where the average resolution curves of the mixed-ADC system with Ternary-ADCs and 1-bit ADCs cross. This means the average resolution of the two systems is the same. Nevertheless, the mixed-ADC system with Ternary-ADCs has a lower iterative decoding threshold. In other words, the mixed-ADC system with Ternary-ADCs has better system performance at the same average resolution. For example, at  $N_L = 12$  and  $N_H = 4$ , the average resolution of the system with the combination of Ternary-ADCs and 4-bit ADCs is the same as the average resolution of the system with the combination of 1-bit ADCs and 5-bit ADCs, around 2 bits/sample. But, at the point  $N_L = 12$  and  $N_H = 4$  in Fig. 6 and Table 2, the iterative decoding threshold of the first system is 2.49 dB and the iterative decoding threshold of the latter is 3.86 dB. This observation suggests that a power gain of about 1.37 dB is obtained if Ternary-ADCs are chosen to use in the low-resolution antenna group.

For a given average resolution, it is more effective to increase the portion of high-resolution antennas than to

increase the resolution of the high-resolution antennas. For example, when the combination of  $N_L = 15$  T-ADCs and  $N_H = 1$  5-bit ADCs results in average resolution of 1.25 bits/sample, the iterative decoding threshold is 2.850 dB. While with the same average resolution, the combination of  $N_L = 13$  T-ADCs and  $N_H = 3$  4-bit ADCs has the iterative decoding of 2.66 dB, or an equivalent gain of 0.19 dB.

In the following section, the simulation is performed to verify the above theoretical observations with a specific protograph LDPC code designed for LS-MIMO communication system with 1-bit ADCs and the finite code length.

## VI. SIMULATION RESULTS

In this section, the proto-matrix of the protograph LDPC code given in (37) is now used to construct a derived LDPC code by performing the copy-and-permutation operation, known as the protograph lifting process. The lifting process is implemented in two steps. In the first lifting step, the protograph is lifted by a factor of 4 using progressive edge growth (PEG) algorithm [35] in order to remove all multiple parallel edges. The second lifting step is determined according to the chosen information block length. In this experiment, protograph has 3 check nodes and 6 variable nodes, the second lifting step is 200, resulting in the information block length of 2400 bits and the equivalent code length is of 4800 bits at the output of the encoder. In the second lifting, the final LDPC code is constructed using the PEG algorithm to determine a circulant permutation of each edge class to avoid short-length cycles occurred within a designed information block length. The coded bit sequence is then modulated with the BPSK scheme, as shown in Fig. 1. The protograph LDPC decoder with a standard message-passing algorithm has a maximum of 50 iterations.

The simulation results of the  $16 \times 16$  MIMO configuration are visually presented in Fig. 9 - Fig. 14. First, let us consider the combination of  $N_L = 15$  low-resolution antennas and  $N_H = 1$  high-resolution antenna. In this considered combination, the majority portion of received antennas with 1-bit ADCs and a minimum number of receive antenna with 5-bit ADC can provide about 0.5 dB power gain, as shown in Fig. 9 and Fig. 10 at the BER or FER level of  $10^{-4}$ . A higher gain is achieved in the combination of Ternary-ADCs with other high-resolution ADCs. At the BER/FER level of  $10^{-4}$ , the power gain of the mixed-ADC system with Ternary-ADCs is about 2.8 dB over the 1-bit ADC system and 2.2 dB over the mixed-ADC system with the combination of 1-bit ADCs and 5-bit ADCs. The gain stems from the increase in the average resolution of the mixed-ADC system with Ternary-ADCs. In particular, the mixed-ADC combination of Ternary-ADCs and 3-bit ADCs has an average resolution of 1.66 bits/sample. While the mixed-ADC combination of 1-bit ADCs and 5-bit ADCs has an average resolution of 1.25 bits/sample. That is equivalent to a 0.41-bits-per-sample increase in the average resolution for an additional gain of 2.2 dB in return. The mentioned

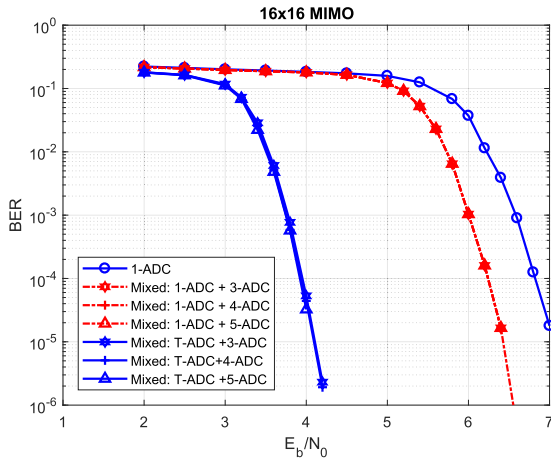


FIGURE 9. BER performance:  $16 \times 16$  MIMO, coding rate  $R = 1/2$ , code length 4800 bits, 50 iterations, mixed-ADC: number of low-resolution antennas  $N_L = 15$ , number of high-resolution antennas  $N_H = 1$ .

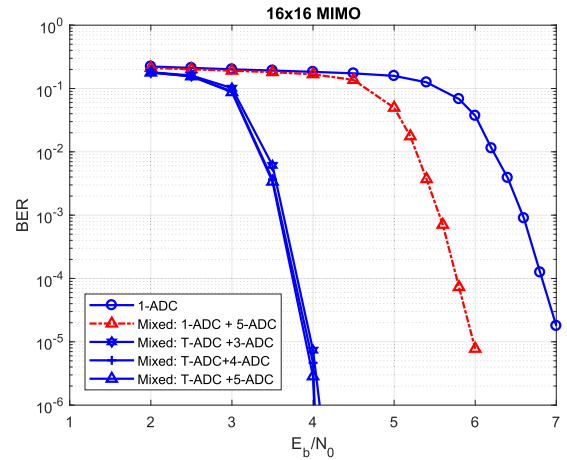


FIGURE 11. BER performance:  $16 \times 16$  MIMO, coding rate  $R = 1/2$ , code length 4800 bits, 50 iterations, mixed-ADC: number of low-resolution antennas  $N_L = 14$ , number of high-resolution antennas  $N_H = 2$ .

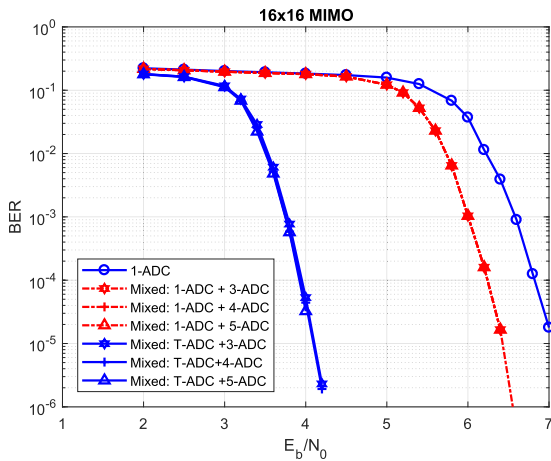


FIGURE 10. FER performance:  $16 \times 16$  MIMO, coding rate  $R = 1/2$ , code length 4800 bits, 50 iterations, mixed-ADC: number of low-resolution antennas  $N_L = 15$ , number of high-resolution antennas  $N_H = 1$ .

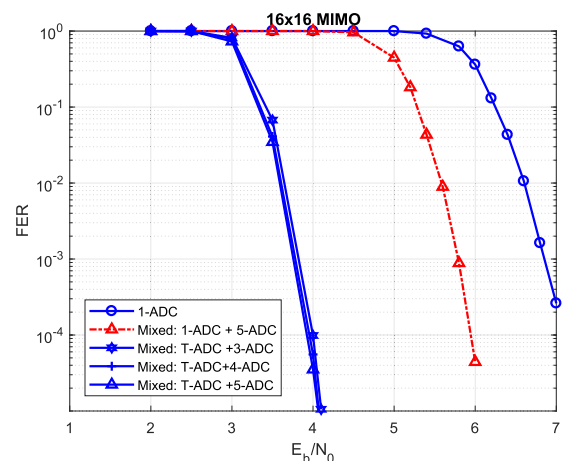


FIGURE 12. FER performance:  $16 \times 16$  MIMO, coding rate  $R = 1/2$ , code length 4800 bits, 50 iterations, mixed-ADC: number of low-resolution antennas  $N_L = 14$ , number of high-resolution antennas  $N_H = 2$ .

gains from simulation results agree with the gains observed from the iterative decoding threshold calculations in the previous section. This means that the proposed Mixed-ADC-LS-MIMO-PEXIT algorithm can provide the performance prediction of protograph LDPC codes with a high level of accuracy.

Consider the same  $16 \times 16$  MIMO configuration but the antenna partition ratio is 1 (i.e.,  $N_L = 8$  and  $N_H = 8$ ), the BER and FER performance curves of different mixed-ADC systems are plotted in Fig. 13 and Fig. 14. The mixed-ADC system, 1-bit ADCs plus 5-bit ADCs, outperforms the uniform 1-bit ADC system with an approximate gain of 3 dB, which is 2.5 dB higher than that of the previous partition ratio of 1/15. The gain observed from the iterative decoding threshold in Table 2 is 2.85 dB. The difference of 0.15 dB between theoretical results and simulation results validates the usefulness of the Mixed-ADC-LS-MIMO PEXIT algorithm in Section IV.E. Plus, the mixed-ADC system based on Ternary-ADCs still gains a power-saving advantage over the mixed-ADC system based

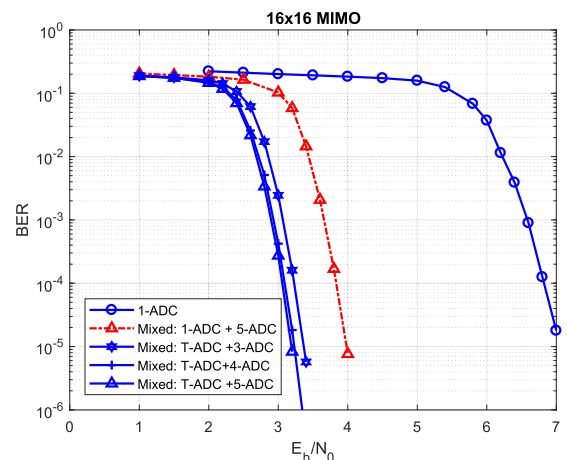
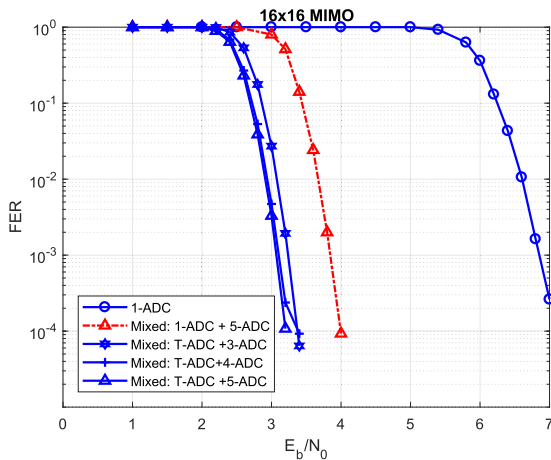
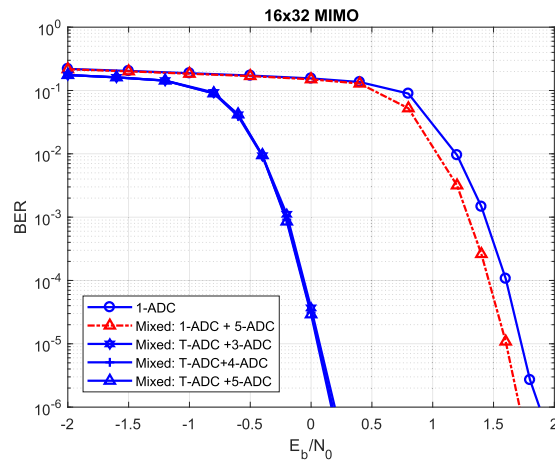


FIGURE 13. BER performance:  $16 \times 16$  MIMO, coding rate  $R = 1/2$ , code length 4800 bits, 50 iterations, mixed-ADC: number of low-resolution antennas  $N_L = 8$ , number of high-resolution antennas  $N_H = 8$ .

on 1-bit ADCs while having lower average resolution. Comparing those two mixed-ADC systems at the BER level



**FIGURE 14.** FER performance:  $16 \times 16$  MIMO, coding rate  $R = 1/2$ , code length 4800 bits, 50 iterations, mixed-ADC: number of low-resolution antennas  $N_L = 8$ , number of high-resolution antennas  $N_H = 8$ .



**FIGURE 15.** BER performance:  $16 \times 32$  MIMO, coding rate  $R = 1/2$ , code length 4800 bits, 50 iterations, mixed-ADC: number of low-resolution antennas  $N_L = 31$ , number of high-resolution antennas  $N_H = 1$ .

of  $10^{-4}$ , the power gain of the Ternary-based mixed-ADC system is 0.6 dB over the 1-bit-based mixed-ADC system while the average resolution of the first system is 2.765 bits/sample (the mix of Ternary-ADCs and 4-bit ADCs) which is 0.235 bits/sample lower than the average resolution of the latter. Referring to the theoretical results in Table 2, the gap between the Ternary-ADC-based system and 1-bit-ADC-based system is 0.72 dB, which is very close to the simulation results. The matching between the theoretical and simulation results confirms the developed theory in Section IV.

The simulation results for the  $16 \times 32$  MIMO configuration with three different antenna partition ratios are shown in Fig. 15 - Fig. 20. Examining the antenna partition ratio of  $1/31$  (i.e.,  $N_L = 31$  and  $N_H = 1$ ), the BER and FER curves are plotted in Fig. 15 and Fig. 16. It is observed that the attainable gain of the 1-bit-based mixed-ADC system over the uniform 1-bit-ADC system is marginal. At the particular BER level of  $10^{-4}$ , the gain is only about 0.1 dB. The theoretical gain of comparing these two systems is 0.135 dB, as shown in Table 3. Contrary to the marginal gain of the 1-bit-based mixed-ADC system, the Ternary-based mixed-ADC system can achieve a gain of 1.6 dB compared to the uniform 1-bit ADC system. This gain again agrees with the theoretical gain of 1.76 dB derived from the iterative decoding thresholds reported in Table 3.

At the higher antenna partition ratio of  $10/22$  (i.e.,  $N_L = 22$ ,  $N_H = 10$ ), the 1-bit-based mixed-ADC system can achieve a bigger gain of around 1.0 dB over the uniform 1-bit ADC system - while the theoretical gain is of 1.241 dB as shown in Table 3. On the other hand, the Ternary-based mixed-ADC system can obtain an additional gain of 1.0 dB over the 1-bit mixed-ADC system. This additional power-saving gain is also confirmed by looking at the theoretical results in Table 3. Particularly, the system with the mix of Ternary-ADCs and 3-bit ADCs has a theoretical gain of 0.836 dB over the system with the mix

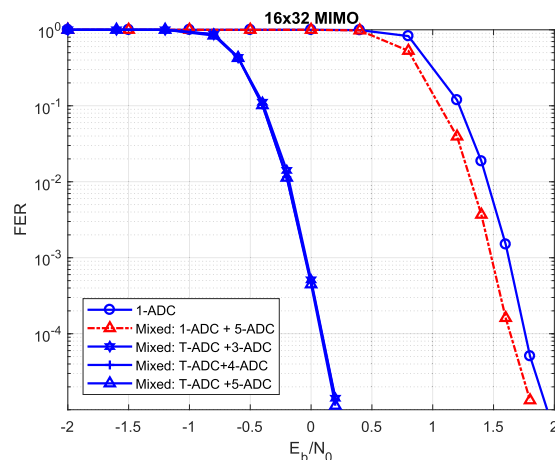


**FIGURE 16.** FER performance:  $16 \times 32$  MIMO, coding rate  $R = 1/2$ , code length 4800 bits, 50 iterations, mixed-ADC: number of low-resolution antennas  $N_L = 31$ , number of high-resolution antennas  $N_H = 1$ .

of 1-bit ADCs and 5-bit ADCs. Remarkably, the average resolution of the combination of Ternary-ADCs and 3-bit ADCs is 1.99 bits/sample, which is 0.26 bits/sample lower than the average resolution combination of 1-bit ADCs and 5-bit ADCs. This observation demonstrates that it is possible to optimize the antenna partition ratio so that the power gain is achieved at a given average resolution by using Ternary-ADCs.

Finally, a crucial observation is that increasing the resolution level for the high-resolution antenna group faces a diminished return effect. That is - observing from both the BER and FER curves from Fig. 9 - Fig. 20, the differences when increasing the resolution level of the high-resolution antenna group from 3 bits to 4 bits or 5 bits are very small. For example, the gap between the curve of Ternary-ADCs combined with 3-bit ADCs and the curve of Ternary-ADCs and 4-bit ADCs is unnoticeable. The theoretical gap derived from iterative decoding threshold data in Table 2 is 0.022 dB - a tiny gap. At the other extreme, for example the  $16 \times 32$

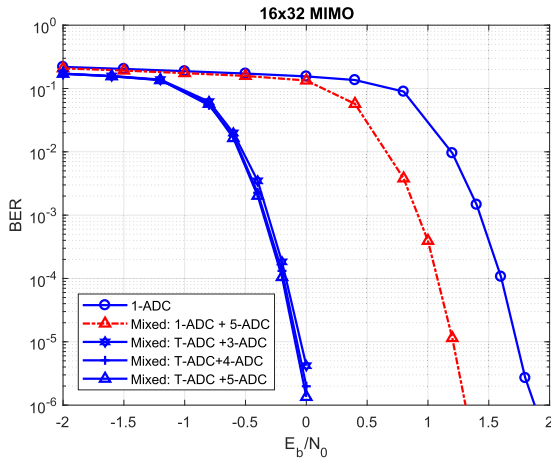


**FIGURE 17.** BER performance:  $16 \times 32$  MIMO, coding rate  $R = 1/2$ , code length 4800 bits, 50 iterations, mixed-ADC: number of low-resolution antennas  $N_L = 24$ , number of high-resolution antennas  $N_H = 8$ .

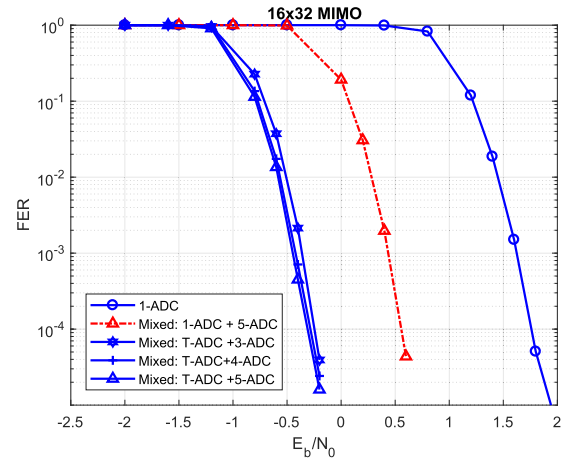


**FIGURE 20.** FER performance:  $16 \times 32$  MIMO, coding rate  $R = 1/2$ , code length 4800 bits, 50 iterations, mixed-ADC: number of low-resolution antennas  $N_L = 22$ , number of high-resolution antennas  $N_H = 10$ .

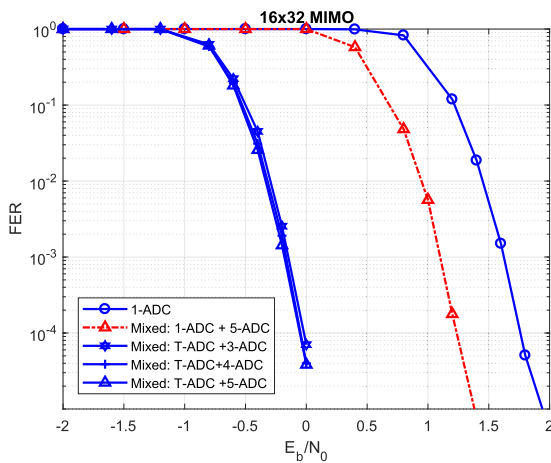


**FIGURE 18.** FER performance:  $16 \times 32$  MIMO, coding rate  $R = 1/2$ , code length 4800 bits, 50 iterations, mixed-ADC: number of low-resolution antennas  $N_L = 24$ , number of high-resolution antennas  $N_H = 8$ .

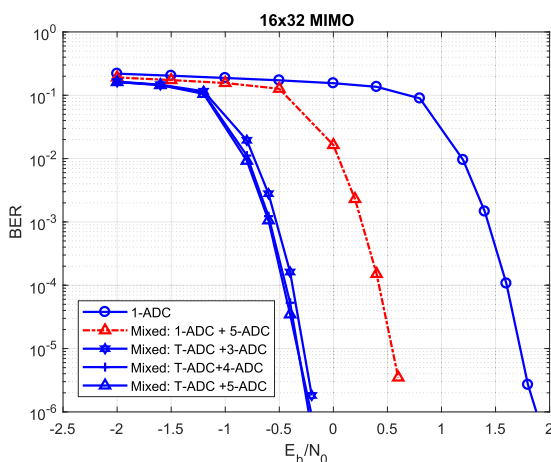


**FIGURE 19.** BER performance:  $16 \times 32$  MIMO, coding rate  $R = 1/2$ , code length 4800 bits, 50 iterations, mixed-ADC: number of low-resolution antennas  $N_L = 22$ , number of high-resolution antennas  $N_H = 10$ .

MIMO configuration with antenna partition ratio of 10/22 in Fig. 19, the gap between two considered systems is a

bit bigger, but it is still considerably small. The theoretical data in Table 3 indicates the fairly small gap of 0.061 dB. This observation implies that 4 or 5 bits seem to be the best resolution level for the high-resolution antenna group, which is contrary to the previous research works where 8 - 10 bits were often used in the high-resolution antenna group. At the same time, Ternary-ADCs should be used to achieve power-saving gains while keeping the average resolution of the mixed-ADC system at the desired level.

### VII. CONCLUSION

In this paper, we derived the joint detection and decoding algorithm on the double-layer graph and the equivalent PEXIT algorithm to assess the performance of the protograph LDPC codes for mixed-ADC LS-MIMO communication systems. The proposed PEXIT algorithm is then used to obtain the performance analysis of the mixed-ADC LS-MIMO systems with a specific protograph LDPC code under various mixed-ADC combination scenarios. The simulation results in two specific MIMO configurations with different antenna partition ratios confirm the accuracy of the proposed Mixed-ADC-LS-MIMO-PEXIT algorithm. In addition, the experiment results show that the mixed-ADC system achieves the highest gain at the extreme point where only one received antenna is equipped with the high-resolution ADCs. Both analytical and simulation results indicate that the maximum resolution level for the high-resolution ADCs is 4 or 5 bits/sample. Beyond this resolution, the additional gain is marginal while the power consumption can be exponentially increased. Remarkably, the mixed-ADC system based on Ternary-ADCs always provides better power-saving gain than the mixed-ADC system based on 1-bit ADCs at the same or even lower average resolution. To improve the system performance further, protograph LDPC codes should be redesigned and/or co-design with the antenna partition ratio parameter to match the variable degree of the proto-matrix with the resolution levels of low-resolution and high-resolution antenna groups.

## REFERENCES

- [1] D. C. Araujo, T. Maksymuk, A. L. F. de Almeida, T. Maciel, J. C. M. Mota, and M. Jo, "Massive MIMO: Survey and future research topics," *IET Commun.*, vol. 10, no. 15, pp. 1938–1946, Oct. 2016.
- [2] K. B. Letaief, W. Chen, Y. Shi, J. Zhang, and Y.-J.-A. Zhang, "The roadmap to 6G: AI empowered wireless networks," *IEEE Commun. Mag.*, vol. 57, no. 8, pp. 84–90, Aug. 2019.
- [3] Z. Zhang, Y. Xiao, Z. Ma, M. Xiao, Z. Ding, X. Lei, G. K. Karagiannidis, and P. Fan, "6G wireless networks: Vision, requirements, architecture, and key technologies," *IEEE Veh. Technol. Mag.*, vol. 14, no. 3, pp. 28–41, Sep. 2019.
- [4] L. Fan, S. Jin, C. K. Wen, and H. Zhang, "Uplink achievable rate for massive MIMO systems with low-resolution ADC," *IEEE Commun. Lett.*, vol. 19, no. 12, pp. 2186–2189, Oct. 2015.
- [5] J. Zhang, L. Dai, X. Li, Y. Liu, and L. Hanzo, "On low-resolution ADCs in practical 5G millimeter-wave massive MIMO systems," *IEEE Commun. Mag.*, vol. 56, no. 7, pp. 205–211, Jul. 2018.
- [6] C. Zhang, Y. Jing, Y. Huang, and X. You, "Massive MIMO with ternary ADCs," *IEEE Signal Process. Lett.*, vol. 27, pp. 271–275, 2020.
- [7] T. Liu, J. Tong, Q. Guo, J. Xi, Y. Yu, and Z. Xiao, "Energy efficiency of massive MIMO systems with low-resolution ADCs and successive interference cancellation," *IEEE Trans. Wireless Commun.*, vol. 18, no. 8, pp. 3987–4002, Aug. 2019.
- [8] J. Dai, J. Liu, J. Wang, J. Zhao, C. Cheng, and J.-Y. Wang, "Achievable rates for full-duplex massive MIMO systems with low-resolution ADCs/DACs," *IEEE Access*, vol. 7, pp. 24343–24353, 2019.
- [9] S. Gao, P. Dong, Z. Pan, and G. Y. Li, "Deep learning based channel estimation for massive MIMO with mixed-resolution ADCs," *IEEE Commun. Lett.*, vol. 23, no. 11, pp. 1989–1993, Nov. 2019.
- [10] L. V. Nguyen, D. T. Ngo, N. H. Tran, A. L. Swindlehurst, and D. H. N. Nguyen, "Supervised and semi-supervised learning for MIMO blind detection with low-resolution ADCs," *IEEE Trans. Wireless Commun.*, vol. 19, no. 4, pp. 2427–2442, Apr. 2020.
- [11] L. Xu, X. Lu, S. Jin, F. Gao, and Y. Zhu, "On the uplink achievable rate of massive MIMO system with low-resolution ADC and RF impairments," *IEEE Commun. Lett.*, vol. 23, no. 3, pp. 502–505, Jan. 2019.
- [12] T. V. Nguyen, H. D. Vu, D. N. Nguyen, and H. T. Nguyen, "Performance analysis of protograph LDPC codes over large-scale MIMO channels with low-resolution ADCs," *IEEE Access*, vol. 7, pp. 145145–145160, 2019.
- [13] Y. Cho and S.-N. Hong, "One-bit successive-cancellation soft-output (OSS) detector for uplink MU-MIMO systems with one-bit ADCs," *IEEE Access*, vol. 7, pp. 27172–27182, 2019.
- [14] F. Mousavi and A. Tadaion, "A simple two-stage detector for massive MIMO systems with one-bit ADCs," in *Proc. 27th Iranian Conf. Electr. Eng. (ICEE)*, Apr. 2019, pp. 1674–1678.
- [15] Q. Bai and J. A. Nossek, "Energy efficiency maximization for 5G multi-antenna receivers," *Trans. Emerg. Telecommun. Technol.*, vol. 26, no. 1, pp. 3–14, Jan. 2015.
- [16] H. N. Dang, T. V. Nguyen, and H. T. Nguyen, "Improve uplink achievable rate for massive MIMO systems with low-resolution ADCs," in *Proc. IEEE 8th Int. Conf. Commun. Electron. (ICCE)*, Jan. 2021, pp. 99–104.
- [17] J. Zhang, L. Dai, Z. He, S. Jin, and X. Li, "Performance analysis of mixed-ADC massive MIMO systems over Rician fading channels," *IEEE J. Sel. Areas Commun.*, vol. 35, no. 6, pp. 1327–1338, Jun. 2017.
- [18] J. Yuan, Q. He, M. Matthaiou, T. Q. S. Quek, and S. Jin, "Toward massive connectivity for IoT in mixed-ADC distributed massive MIMO," *IEEE Internet Things J.*, vol. 7, no. 3, pp. 1841–1856, Mar. 2020.
- [19] J. Liu, J. Xu, W. Xu, S. Jin, and X. Dong, "Multiuser massive MIMO relaying with mixed-ADC receiver," *IEEE Signal Process. Lett.*, vol. 24, no. 1, pp. 76–80, Dec. 2016.
- [20] D. Tse and P. Viswanath, *Fundamentals Of Wireless Communication*. Cambridge, U.K.: Cambridge Univ. Press, 2005.
- [21] M. Srinivasan and S. Kalyani, "Analysis of massive MIMO with low-resolution ADC in Nakagami- $m$  fading," *IEEE Commun. Lett.*, vol. 23, no. 4, pp. 764–767, Apr. 2019.
- [22] H. T. Nguyen, T. A. Ramstad, and I. Balasingham, "Wireless sensor communication system based on direct-sum source coder," *IET Wireless Sensor Syst.*, vol. 1, no. 2, pp. 96–104, Jun. 2011.
- [23] D. Hui and D. L. Neuhoff, "Asymptotic analysis of optimal fixed-rate uniform scalar quantization," *IEEE Trans. Inf. Theory*, vol. 47, no. 3, pp. 957–977, Mar. 2001.
- [24] T. Takahashi, S. Ibi, and S. Sampei, "On normalization of matched filter belief in GABP for large MIMO detection," in *Proc. IEEE 84th Veh. Technol. Conf. (VTC-Fall)*, Sep. 2016, pp. 1–6.
- [25] W. Fukuda, T. Abiko, T. Nishimura, T. Ohgane, Y. Ogawa, Y. Ohwatari, and Y. Kishiyama, "Low-complexity detection based on belief propagation in a massive MIMO system," in *Proc. IEEE 77th Veh. Technol. Conf. (VTC Spring)*, Jun. 2013, pp. 1–5.
- [26] T. J. Richardson, M. A. Shokrollahi, and R. L. Urbanke, "Design of capacity-approaching irregular low-density parity-check codes," *IEEE Trans. Inf. Theory*, vol. 47, no. 2, pp. 619–637, Feb. 2001.
- [27] S. ten Brink, G. Kramer, and A. Ashikhmin, "Design of low-density parity-check codes for modulation and detection," *IEEE Trans. Commun.*, vol. 52, no. 4, pp. 670–678, Apr. 2004.
- [28] G. Liva and M. Chiani, "Protograph LDPC codes design based on EXIT analysis," in *Proc. IEEE Global Telecommun. Conf. (GLOBECOM)*, Nov. 2007, pp. 3250–3254.
- [29] Y. Fang, P. Chen, L. Wang, F. C. M. Lau, and K. K. Wong, "Performance analysis of protograph-based low-density parity-check codes with spatial diversity," *IET Commun.*, vol. 6, no. 17, pp. 2941–2948, Nov. 2012.
- [30] H. D. Vu, T. V. Nguyen, D. N. Nguyen, and H. T. Nguyen, "On design of protograph LDPC codes for large-scale MIMO systems," *IEEE Access*, vol. 8, pp. 46017–46029, 2020.
- [31] T. V. Nguyen and A. Nosratinia, "Rate-compatible short-length protograph LDPC codes," *IEEE Commun. Lett.*, vol. 17, no. 5, pp. 948–951, May 2013.
- [32] T. Van Nguyen and H. T. Nguyen, "The design of optimized fast decoding protograph LDPC codes," in *Proc. Int. Conf. Adv. Technol. Commun. (ATC)*, Oct. 2016, pp. 282–286.
- [33] T. Abiko, W. Fukuda, T. Nishimura, T. Ohgane, Y. Ogawa, Y. Ohwatari, and Y. Kishiyama, "An EXIT chart analysis for belief-propagation based detection in a large-scale MIMO system," in *Proc. IEEE 77th Veh. Technol. Conf. (VTC Spring)*, Jun. 2013, pp. 1–5.
- [34] H. N. Dang and T. V. Nguyen, "Protograph LDPC code design for LS-MIMO 1-bit ADC systems," *REV J. Electron. Commun.*, vol. 11, pp. 1–7, May 2021.
- [35] X.-Y. Hu, E. Eleftheriou, and D. M. Arnold, "Regular and irregular progressive edge-growth tanner graphs," *IEEE Trans. Inf. Theory*, vol. 51, no. 1, pp. 386–398, Jan. 2005.



**HUNG N. DANG** received the B.Sc. and M.Sc. degrees in information technology from the Posts and Telecommunications Institute of Technology (PTIT), Hanoi, Vietnam, where he is currently pursuing the Ph.D. degree in information systems and wireless communications. His research interests include massive MIMO communications, channel coding design and analysis, and wireless sensor networks.



**HIEU T. NGUYEN** received the B.Sc. degree in electrical engineering from the Hanoi University of Science and Technology, the M.Sc. degree in electrical engineering from the University of Saskatchewan, Canada, and the Ph.D. degree in electrical engineering from the Norwegian University of Science and Technology. He is currently a Faculty Member of the Faculty of Technology, Natural Sciences, and Maritime Sciences, University of South-Eastern Norway (USN).



**THUY V. NGUYEN** received the B.Sc. degree in electrical engineering from the Hanoi University of Science and Technology (HUST), Hanoi, Vietnam, the M.Sc. degree in electrical engineering from New Mexico State University, Las Cruces, NM, USA, and the Ph.D. degree in electrical engineering from The University of Texas at Dallas, Richardson, TX, USA. He was a member of the Technical Staff with Flash Channel Architecture, Seagate, Fremont, CA, USA. He is currently a Lecturer with the Faculty of Information Technology, Posts and Telecommunications Institute of Technology (PTIT), Hanoi. His research interest includes coding theory and its applications in next generation communication systems.